Lorentz and *CPT* violation in neutrinos

V. Alan Kostelecký and Matthew Mewes
Physics Department, Indiana University, Bloomington, Indiana 47405, USA
(Received 2 September 2003; published 30 January 2004)

A general formalism is presented for violations of Lorentz and *CPT* symmetry in the neutrino sector. The effective Hamiltonian for neutrino propagation in the presence of Lorentz and *CPT* violation is derived, and its properties are studied. Possible definitive signals in existing and future neutrino-oscillation experiments are discussed. Among the predictions are direction-dependent effects, including neutrino-antineutrino mixing, sidereal and annual variations, and compass asymmetries. Other consequences of Lorentz and *CPT* violation involve unconventional energy dependences in oscillation lengths and mixing angles. A variety of simple models both with and without neutrino masses are developed to illustrate key physical effects. The attainable sensitivities to coefficients for Lorentz violation in the Standard-Model Extension are estimated for various types of experiments. Many experiments have potential sensitivity to Planck-suppressed effects, comparable to the best tests in other sectors. The lack of existing experimental constraints, the wide range of available coefficient space, and the variety of novel effects imply that some or perhaps even all of the existing data on neutrino oscillations might be due to Lorentz and *CPT* violation.

DOI: 10.1103/PhysRevD.69.016005 PACS number(s): 11.30.Cp, 11.30.Er, 14.60.Pq

I. INTRODUCTION

The minimal Standard Model (SM) of particle physics offers a successful description of most processes in nature but leaves unresolved several experimental and theoretical issues. On the experimental front, observations of neutrino oscillations have accumulated convincing evidence that the description of physical properties of neutrinos requires modification of the neutrino sector in the minimal SM. Most experimental results to date can be described theoretically by adding neutrino masses to the minimal SM, but a complete understanding of the existing data awaits further experimentation. On the theoretical front, the SM is expected to be the low-energy limit of a more fundamental theory that unifies quantum physics and gravity at the Planck scale $m_P \simeq 10^{19}$ GeV. Direct measurements at this energy scale are impractical, but suppressed low-energy signatures from the anticipated new physics might be detectable in sensitive existing experiments.

In this work, we address both these topics by studying effects on the neutrino sector of relativity violations, a promising class of Planck-scale signals. These violations might arise through the breaking of Lorentz symmetry and perhaps also the breaking of *CPT* symmetry [1]. Since the SM is known to provide a successful description of most physics at low energies compared to the Planck scale, any such signals must appear at low energies in the form of an effective quantum field theory containing the SM. The general effective quantum field theory constructed from the SM and allowing arbitrary coordinate-independent Lorentz violation is called the Standard-Model Extension (SME) [2]. It provides a link to the Planck scale through operators of nonrenormalizable dimension [3,4]. Since *CPT* violation implies Lorentz violation [5], this theory also allows for general *CPT* breaking. The SME therefore provides a realistic theoretical basis for studies of Lorentz violation, with or without *CPT* breaking.

The Lagrangian of the SME consists of the usual SM Lagrangian supplemented by all possible terms that can be constructed with SM fields and that introduce violations of Lorentz symmetry. The additional terms have the form of Lorentz-violating operators coupled to coefficients with Lorentz indices, and they could arise in a variety of ways. One generic and elegant mechanism is spontaneous Lorentz violation, proposed first in string theory and field theories with gravity [6] and then generalized to include *CPT* violation [7]. Another popular framework for Lorentz violation is noncommutative field theory, in which realistic models form a subset of the SME involving operators of nonrenormalizable dimension [8]. Other proposed sources of Lorentz and *CPT* violation include various nonstring approaches to quantum gravity [9], random dynamics [10], and multiverses [11]. Planck-scale sensitivity to the coefficients for Lorentz violation in the SME has been achieved in various experiments, including ones with mesons [3,12,13], baryons [14–16], electrons [17,18], photons [19–22], and muons [23]. However, no experiments to date have measured neutrino-sector coefficients for Lorentz violation.

Here, we explore neutrino behavior in the presence of Lorentz and *CPT* violation using the SME framework. The original proposal for Lorentz and *CPT* violation in neutrinos [2] has since been followed by several theoretical investigations within the context of the SME [24–29], most of which have chosen to restrict attention to a small number of coefficients. A comprehensive theoretical study of Lorentz and CPT violation in neutrinos has been lacking. The present work partially fills this gap by applying the ideas of the SME to a general neutrino sector with all possible couplings of left- and right-handed neutrinos and with sterile neutrinos. We concentrate mostly on Lorentz-violating operators of renormalizable dimension, which dominate the low-energy physics in typical theories, but some generic consequences of Lorentz-violating operators of nonrenormalizable dimension are also considered [3,4,30]. The effective Hamiltonian describing free neutrino propagation is obtained, and its implications are studied. The formalism presented in this work thereby provides a general theoretical basis for future studies

of Lorentz and CPT violation in neutrinos. We also illustrate various key physical ideas of Lorentz and *CPT* violation through simple models, and we discuss experimental signals. Our primary focus here is on oscillation data [31], but the formalism is applicable also to other types of experiments including direct mass searches [32], neutrinoless double-beta decay [33], and supernova neutrinos [34].

Several features of Lorentz and CPT violation that we uncover are common to other sectors of the SME, including unconventional energy dependence and dependence on the direction of propagation. We also find that Lorentz-violating neutrino-antineutrino mixing with lepton-number violation naturally arises from Majorana-like couplings. These features lead to several unique signals for Lorentz and *CPT* violation. For example, the direction dependence potentially generates sidereal variations in terrestrial experiments as the Earth rotates, annual variations in solar-neutrino properties, and intrinsic differences in neutrino flux from different points on the compass or different angular heights at the location of the detector. The unconventional energy dependence produces a variety of interesting potential signals, including resonances in the vacuum [25,29] as well as the usual Mikheyev-Smirnov-Wolfenstein (MSW) resonances in matter [35].

Experiments producing evidence for neutrino oscillations to date include atmospheric-neutrino experiments [36], solar-neutrino experiments [37–42], reactor experiments [43], and accelerator-based experiments [44,45]. Most current data are consistent with the introduction of three massive-neutrino states, usually attributed to Grand-Unified-Theory (GUT) scale physics. However, as we demonstrate in this work, the possibility remains that the observed neutrino oscillations may be due at least in part and conceivably even entirely to Lorentz and CPT violation from the Planck scale. In any event, experiments designed to test neutrino mass are also well suited for tests of Lorentz and CPT invariance, and they have the potential to produce the first measurements of violations of these fundamental symmetries, signaling possible Planck-scale physics.

The organization of this paper is as follows. Section II presents the basic theory and definitions, obtaining the effective Hamiltonian for neutrino propagation and discussing its properties. Issues of experimental sensitivities and possible constraints from experiments in other sectors are considered in Sec. III. Certain key features of neutrino behavior in the presence of Lorentz and CPT violation are illustrated in the sample models of Sec. IV. Some remarks about both generic and experiment-specific predictions are provided in Sec. V. Throughout, we follow the notation and conventions of Refs. [2,4].

II. THEORY

A. Basics

Our starting point is a general theory describing N neutrino species. The theory is assumed to include all possible Majorana- and Dirac-type couplings of left- and right-handed neutrinos, including Lorentz- and *CPT*-violating ones. The neutrino sector of the minimal SME is therefore included, along with other terms such as those involving right-handed neutrinos.

We denote the neutrino fields by the set of Dirac spinors $\{\nu_e,\nu_\mu,\nu_\tau,\ldots\}$ and their charge conjugates by $\{\nu_{eC}\equiv\nu_e^C,\ \nu_{\mu C}\equiv\nu_\mu^C,\ \nu_{\tau C}\equiv\nu_\tau^C,\ \ldots\}$, where charge conjugation of a Dirac spinor is defined as usual: $\nu_a^C\equiv C\overline{\nu}_a^T$. By definition, active neutrinos are detected via weak interactions with left-handed components of $\{\nu_e,\nu_\mu,\nu_\tau\}$. Complications may arise in the full SME, where Lorentz-violating terms alter these interactions and can modify the detection process. However, such modifications are expected to be tiny and well beyond the sensitivity of current experiments. In contrast, propagation effects can become appreciable for large baselines. We therefore focus in this work on solutions to the Lorentz-violating equations of motion that describe free propagation of the N neutrino species.

It is convenient to place all the fields and their conjugates into a single object ν_A, where the index A ranges over the $2N$ possibilities $\{e,\mu,\tau,\ldots,e^C,\mu^C,\tau^C,\ldots\}$. This setup allows us to write the equations of motion in a form analogous to the Lorentz-violating QED extension [2,4], and it can readily accommodate Dirac, Majorana, or more general types of neutrinos. Our explicit analysis in this section is performed under the assumption that Lorentz-violating operators of renormalizable dimension dominate the low-energy physics. Then, the general equations of motion for free propagation can be written as a first-order differential operator acting on the object ν_A:

$$(i\Gamma^\nu_{AB}\partial_\nu - M_{AB})\,\nu_B = 0. \tag{1}$$

Here, each constant quantity Γ^μ_{AB}, M_{AB} is also a 4×4 matrix in spinor space. Note that the usual equations of motion for Dirac and Majorana neutrinos are special cases of this equation.

The matrices Γ^μ_{AB} and M_{AB} can be decomposed using the basis of γ matrices. We define

$$\begin{aligned}\Gamma^\nu_{AB} &\equiv \gamma^\nu\delta_{AB} + c^{\mu\nu}_{AB}\gamma_\mu + d^{\mu\nu}_{AB}\gamma_5\gamma_\mu \\ &\quad + e^\nu_{AB} + if^\nu_{AB}\gamma_5 + \frac{1}{2}g^{\lambda\mu\nu}_{AB}\sigma_{\lambda\mu},\\ M_{AB} &\equiv m_{AB} + im_{5AB}\gamma_5 + a^\mu_{AB}\gamma_\mu \\ &\quad + b^\mu_{AB}\gamma_5\gamma_\mu + \frac{1}{2}H^{\mu\nu}_{AB}\sigma_{\mu\nu}.\end{aligned} \tag{2}$$

In these equations, the masses m and m_5 are Lorentz and *CPT* conserving. The coefficients c,d,H are *CPT* conserving but Lorentz violating, while a, b, e, f, g are both *CPT* and Lorentz violating. Requiring hermiticity of the theory imposes the conditions $\Gamma^\nu_{AB}=\gamma^0(\Gamma^\nu_{BA})^\dagger\gamma^0$ and $M_{AB}=\gamma^0(M_{BA})^\dagger\gamma^0$, which implies all coefficients are hermitian in generation space.

The above construction carries some redundancies that stem from the interdependence of ν and ν^C. This implies certain symmetries for Γ^ν and M. Note first that charge con-

jugation can be written as a linear transformation on ν_A: $\nu_A^C = \mathcal{C}_{AB}\nu_B$, where $\mathcal{C}$ is the symmetric matrix with nonzero elements $\mathcal{C}_{ee^C} = \mathcal{C}_{\mu\mu^C} = \mathcal{C}_{\tau\tau^C} = \cdots = 1$. Then, in terms of $\mathcal{C}$ and the spinor matrix C, the interdependence of ν and ν^C implies the relations

$$\Gamma^{\nu}_{AB} = -\mathcal{C}_{AC}\mathcal{C}_{BD}C(\Gamma^{\nu}_{DC})^T C^{-1},$$
$$M_{AB} = \mathcal{C}_{AC}\mathcal{C}_{BD}C(M_{DC})^T C^{-1}, \tag{3}$$

where the transpose T acts in spinor space. Suppressing generation indices, this translates to

$$c^{\mu\nu} = \mathcal{C}(c^{\mu\nu})^T\mathcal{C}, \quad m = \mathcal{C}(m)^T\mathcal{C},$$
$$d^{\mu\nu} = -\mathcal{C}(d^{\mu\nu})^T\mathcal{C}, \quad m_5 = \mathcal{C}(m_5)^T\mathcal{C},$$
$$e^{\nu} = -\mathcal{C}(e^{\nu})^T\mathcal{C}, \quad a^{\nu} = -\mathcal{C}(a^{\nu})^T\mathcal{C},$$
$$f^{\nu} = -\mathcal{C}(f^{\nu})^T\mathcal{C}, \quad b^{\nu} = \mathcal{C}(b^{\nu})^T\mathcal{C},$$
$$g^{\lambda\mu\nu} = \mathcal{C}(g^{\lambda\mu\nu})^T\mathcal{C}, \quad H^{\mu\nu} = -\mathcal{C}(H^{\mu\nu})^T\mathcal{C}, \tag{4}$$

where now the transpose T acts in generation space. Note that the overall signs in the above equations are chosen to match their derivation within the conventional lagrangian formalism involving anticommuting fermion fields.

Equation (1) provides a basis for a general Lorentz- and *CPT*-violating relativistic quantum mechanics of freely propagating neutrinos. However, the unconventional time-derivative term complicates the construction of the corresponding Hamiltonian. This difficulty also arises in the minimal QED extension, but it may be overcome [4] if there exists a nonsingular matrix A satisfying the relationship $A^\dagger\gamma^0\Gamma^0 A = 1$. The field redefinition $\nu_A = A_{AB}\chi_B$ then allows the equations of motion (1) to be written as $(i\delta_{AB}\partial_0 - \mathcal{H}_{AB})\chi_B = 0$, where the Hamiltonian is given by $\mathcal{H} = -A^\dagger\gamma^0(i\Gamma^j\partial_j - M)A$.

Denoting $\delta\Gamma^\nu$ and δM as the Lorentz-violating portions of Γ^ν and M, and under the reasonable assumption that $|\delta\Gamma^0| < 1$, a satisfactory field redefinition is given by the power series $A = (1+\gamma^0\delta\Gamma^0)^{-1/2} = 1 - \frac{1}{2}\gamma^0\delta\Gamma^0 + \cdots$. Separating the Hamiltonian $\mathcal{H}$ into a Lorentz-conserving part $\mathcal{H}_0$ and a Lorentz-violating part $\delta\mathcal{H}$, which we assume is small relative to $\mathcal{H}_0$, we can use the above expression for A to obtain an expansion of $\delta\mathcal{H}$ in terms of $\mathcal{H}_0$ and coefficients for Lorentz violation. Explicitly, at leading order in coefficients for Lorentz violation, we obtain

$$\delta\mathcal{H} = -\frac{1}{2}(\gamma^0\delta\Gamma^0\mathcal{H}_0 + \mathcal{H}_0\gamma^0\delta\Gamma^0) - \gamma^0(i\delta\Gamma^j\partial_j - \delta M). \tag{5}$$

This expression is therefore the basis for a general study of leading-order Lorentz and *CPT* violation in the neutrino sector.

At this stage, prior to beginning our study of Eq. (5), it is useful to review the properties of the Lorentz-conserving Hamiltonian [46,47]

$$\mathcal{H}_0 = -\gamma^0(i\gamma^j\partial_j - M_0). \tag{6}$$

The Lorentz-conserving dynamics is completely determined by the mass matrix M_0, which in its general form can be written

$$M_0 = m + im_5\gamma_5 = m_L P_L + m_R P_R \tag{7}$$

with $m_R = (m_L)^\dagger = m + im_5$ and $P_L = \frac{1}{2}(1-\gamma_5), P_R = \frac{1}{2}(1+\gamma_5)$. The components of the matrix $m_R = m_L^\dagger$ can be identified with Dirac- or Majorana-type masses by separating m_R into four $N\times N$ submatrices. It is often encountered in the form of the symmetric matrix

$$m_R\mathcal{C} = \begin{pmatrix} L & D \\ D^T & R \end{pmatrix}. \tag{8}$$

The matrices R and L are the right- and left-handed Majorana-mass matrices, while D is the Dirac-mass matrix. In general, R, L and D are complex matrices restricted only by the requirement that R and L are symmetric. Note that a left-handed Majorana coupling is incompatible with electroweak-gauge invariance. In contrast, Dirac and right-handed Majorana couplings can preserve the usual gauge invariance.

It is always possible to find a basis in which the mass matrix M_0 is diagonal. Labeling the fields in this basis by $\chi_{A'}$, where $A' = 1, \ldots, 2N$, then the unitary transformation relating the two bases can be written as

$$U_{A'A} = V_{A'A}P_L + (V\mathcal{C})^*_{A'A}P_R, \tag{9}$$

where V is a $2N\times 2N$ unitary matrix. Here, it is understood that $U_{A'A}$ carries spinor indices that have been suppressed. In the new basis, the mass matrix $m_{LA'B'} = m_{RA'B'} = m_{(A')}\delta_{A'B'}$ is diagonal with real non-negative entries. The neutrinos $\chi_{A'} = \chi^C_{A'} = V_{A'A}P_L\chi_A + V^*_{A'A}P_R\chi^C_A$ are Majorana particles, regardless of the form of M_0.

B. Effective Hamiltonian

The discussion above applies to an arbitrary number of neutrino species and an arbitrary mass spectrum. Since a general treatment is rather cumbersome, we restrict attention in what follows to the minimal physically reasonable extension with $N=3$. For definiteness, we also assume a standard seesaw mechanism [48] with the components of R much larger than those of D or L. This mechanism suppresses the propagation of right-handed neutrinos, so the analysis below also contains other Lorentz- and CPT-violating scenarios dominated by light or massless left-handed neutrinos, including the minimal SME.

Ordering the masses $m_{(A')}$ from smallest to largest, we assume that $m_{(1)}, m_{(2)}, m_{(3)}$ are small compared to the neutrino energies and possibly zero, and that the remaining masses $m_{(4)}, m_{(5)}, m_{(6)}$ are large with the corresponding energy eigenstates kinematically forbidden. In this situation the submatrix $V_{a'a}$, where $a = e, \mu, \tau$ and $a' = 1,2,3$, is approximately unitary.

To aid in solving the equations of motion, we define

$$\chi_A(t;\vec{x}) = \int \frac{d^3p}{(2\pi)^3}\chi_A(t;\vec{p})e^{i\vec{p}\cdot\vec{x}},$$

$$\begin{aligned}\chi_A(t;\vec{p}) = {} & b_A(t;\vec{p})u_L(\vec{p}) + (\mathcal{C}d)_A(t;\vec{p})u_R(\vec{p}) \\ & + (\mathcal{C}b)^*_A(t;-\vec{p})v_R(-\vec{p}) \\ & + d^*_A(t;-\vec{p})v_L(-\vec{p}).\end{aligned} \tag{10}$$

This is chosen to satisfy explicitly the charge-conjugation condition $\chi^C_A = \mathcal{C}_{AB}\chi_B$. The spinor basis $\{u_L(\vec{p}), u_R(\vec{p}), v_R(-\vec{p}), v_L(-\vec{p})\}$ obeys the usual relations for massless fermions, with $v_{R,L}(\vec{p}) = C\overline{u}^T_{L,R}(\vec{p})$. It has eigenvalues of the helicity operator $\gamma_5\gamma^0\vec{\gamma}\cdot\vec{p}/|\vec{p}|$ given by $\{-,+,-,+\}$ and eigenvalues of the chirality operator γ_5 given by $\{-,+,+,-\}$. For simplicity, we normalize with $u^\dagger_\alpha u_\beta = v^\dagger_\alpha v_\beta = \delta_{\alpha\beta}$ for $\alpha,\beta = L,R$. The definition (10) implies that the amplitudes $b_{e,\mu,\tau}$ may be approximately identified with active neutrinos and $d_{e,\mu,\tau}$ with active antineutrinos. The remaining amplitudes b_{e^C,μ^C,τ^C} and d_{e^C,μ^C,τ^C} cover the space of sterile right-handed neutrinos, but a simple identification with flavor neutrinos and antineutrinos would be inappropriate in view of their large mass.

In the mass-diagonal Majorana basis, we restrict attention to the propagating states consisting of the light neutrinos. Taking the Hamiltonian in this basis

$$\mathcal{H}_{a'b'}(\vec{p}) = \gamma^0(\vec{\gamma}\cdot\vec{p} + m_{(a')})\delta_{a'b'} + \delta\mathcal{H}_{a'b'}(\vec{p}), \tag{11}$$

and applying it to $\chi_{b'}(t;\vec{p}) = U_{b'B}\chi_B(t;\vec{p})$ yields the equations of motion in terms of the amplitudes b and d. The result takes the form of the matrix equation

$$[i\delta_{a'b'}\partial_0 - H_{a'b'}(\vec{p})]\begin{pmatrix} b_{b'}(t;\vec{p}) \\ d_{b'}(t;\vec{p}) \\ b^*_{b'}(t;-\vec{p}) \\ d^*_{b'}(t;-\vec{p})\end{pmatrix} = 0, \tag{12}$$

where for convenience we have defined $b_{b'} = V_{b'B}b_B$ and $d_{b'} = V^*_{b'B}d_B$, and where $H_{a'b'}$ is the spinor-decomposed form of $\mathcal{H}_{a'b'}$.

The propagation of kinematically allowed states is completely determined by the amplitudes $b_{a'}$ and $d_{a'}$. However, for purposes of comparison with experiment it is convenient to express the result using the amplitudes associated with active neutrinos, $b_{e,\mu,\tau}$ and $d_{e,\mu,\tau}$. The relevant calculation is somewhat lengthy and is deferred to Appendix A. It assumes that the submatrix $V_{a'a}$ is unitary, and it neglects terms that enter as small masses $m_{(a')}$ multiplied by coefficients for Lorentz violation, since these are typically suppressed. The calculation reveals that the time evolution of the active-neutrino amplitudes is given by the equation

$$\begin{pmatrix} b_a(t;\vec{p}) \\ d_a(t;\vec{p})\end{pmatrix} = \exp(-ih_{\rm eff}t)_{ab}\begin{pmatrix} b_b(0;\vec{p}) \\ d_b(0;\vec{p})\end{pmatrix}, \tag{13}$$

where $h_{\rm eff}$ is the effective Hamiltonian describing flavor neutrino propagation. To leading order, it is given by

$$\begin{aligned}(h_{\rm eff})_{ab} = {} & |\vec{p}|\,\delta_{ab}\begin{pmatrix}1 & 0\\ 0 & 1\end{pmatrix} + \frac{1}{2|\vec{p}|}\begin{pmatrix}(\tilde{m}^2)_{ab} & 0\\ 0 & (\tilde{m}^2)^*_{ab}\end{pmatrix} \\ & + \frac{1}{|\vec{p}|}\begin{pmatrix}[(a_L)^\mu p_\mu - (c_L)^{\mu\nu}p_\mu p_\nu]_{ab} & -i\sqrt{2}p_\mu(\epsilon_+)_\nu[(g^{\mu\nu\sigma}p_\sigma - H^{\mu\nu})\mathcal{C}]_{ab} \\ i\sqrt{2}p_\mu(\epsilon_+)^*_\nu[(g^{\mu\nu\sigma}p_\sigma + H^{\mu\nu})\mathcal{C}]^*_{ab} & [-(a_L)^\mu p_\mu - (c_L)^{\mu\nu}p_\mu p_\nu]^*_{ab}\end{pmatrix},\end{aligned} \tag{14}$$

where we have defined $(c_L)^{\mu\nu}_{ab} \equiv (c+d)^{\mu\nu}_{ab}$ and $(a_L)^\mu_{ab} \equiv (a+b)^\mu_{ab}$ for reasons explained below. The approximate four momentum p_μ may be taken as $p_\mu = (|\vec{p}|;-\vec{p})$ at leading order. The Lorentz-conserving mass term results from the usual seesaw mechanism with $\tilde{m}^2 \equiv m_l m_l^\dagger$, where m_l is the light-mass matrix $m_l = L - DR^{-1}D^T$. The complex vector $(\epsilon_+)_\mu$ satisfies the conditions

$$\begin{aligned}p^\mu(\epsilon_+)^\nu - p^\nu(\epsilon_+)^\mu &= i\epsilon^{\mu\nu\rho\sigma}p_\rho(\epsilon_+)_\sigma, \\ (\epsilon_+)^\nu(\epsilon_+)^*_\nu &= -1.\end{aligned} \tag{15}$$

A suitable choice is $(\epsilon_+)^\nu = (1/\sqrt{2})(0;\hat{\epsilon}_1 + i\hat{\epsilon}_2)$, where $\hat{\epsilon}_1, \hat{\epsilon}_2$ are real and $\{\vec{p}/|\vec{p}|, \hat{\epsilon}_1, \hat{\epsilon}_2\}$ form a right-handed orthonormal triad. Note that $(\epsilon_+)^\nu$ and $(\epsilon_-)^\nu \equiv (\epsilon_+)^{\nu *}$ is analogous to the usual photon helicity basis. The appearance of these vectors reflects the near-definite helicity of active neutrinos. The vectors $\hat{\epsilon}_1$ and $\hat{\epsilon}_2$ can be arbitrarily set by rotations or equivalently by multiplying $(\epsilon_+)^\nu$ by a phase, which turns out to be equivalent to changing the relative phase between the basis spinors u_L and u_R.

Only the diagonal kinetic term in $h_{\rm eff}$ arises in the minimal SM. The term involving $(\tilde{m}^2)_{ab}$ encompasses the usual massive-neutrino case without sterile neutrinos. The leading-order Lorentz-violating contributions to neutrino-neutrino mixing are controlled by the coefficient combinations $(a+b)^\mu_{ab}$ and $(c+d)^{\mu\nu}_{ab}$. These combinations conserve the usual SU(3)×SU(2)×U(1) gauge symmetry and correspond to the coefficients $(a_L)^\mu_{ab}$ and $(c_L)^{\mu\nu}_{ab}$ in the minimal SME. Note that the orthogonal combinations $(a-b)^\mu_{ab}$ and

$(c-d)^{\mu\nu}_{ab}$ also conserve the usual gauge symmetry, but they correspond to self-couplings of right-handed neutrinos and are therefore irrelevant for leading-order processes involving active neutrinos. The remaining coefficients $(g^{\mu\nu\sigma}\mathcal{C})_{ab}$ and $(H^{\mu\nu}\mathcal{C})_{ab}$ appear in $h_{\rm eff}$ through Majorana-like couplings that violate $\mathrm{SU}(3)\times\mathrm{SU}(2)\times\mathrm{U}(1)$ gauge invariance and lepton-number conservation. They generate Lorentz-violating neutrino-antineutrino mixing.

Some combinations of coefficients may be unobservable, either due to symmetries or because they can be removed through field redefinitions [2,4,49,50]. For example, the trace component $\eta_{\mu\nu}(c_L)^{\mu\nu}$ is Lorentz invariant and can be absorbed into the usual kinetic term, so it may be assumed zero for convenience. In fact, even if this combination is initially nonzero, it remains absent from the leading-order effective Hamiltonian because the trace of $p_\mu p_\nu$ vanishes. Other examples of unobservable coefficients include certain combinations of $g^{\mu\nu\sigma}$ and $H^{\mu\nu}$. The antisymmetry properties $g^{\mu\nu\sigma}=-g^{\nu\mu\sigma}$, $H^{\mu\nu}=-H^{\nu\mu}$ and the properties of $(\epsilon_+)_\nu$ can be combined to prove that the physically significant combinations of $g^{\mu\nu\sigma}$ and $H^{\mu\nu}$ are given by the relations

$$p_\mu(\epsilon_+)_\nu g^{\mu\nu\sigma}=|\vec{p}|(\epsilon_+)_\nu\tilde{g}^{\nu\sigma},$$

$$p_\mu(\epsilon_+)_\nu H^{\mu\nu}=|\vec{p}|(\epsilon_+)_\nu\tilde{H}^{\nu}, \tag{16}$$

where we have defined

$$\tilde{g}^{\nu\sigma}\equiv g^{0\nu\sigma}+\frac{i}{2}\epsilon^{0\nu}{}_{\gamma\rho}g^{\gamma\rho\sigma},$$

$$\tilde{H}^{\nu}\equiv H^{0\nu}+\frac{i}{2}\epsilon^{0\nu}{}_{\gamma\rho}H^{\gamma\rho}. \tag{17}$$

Only these combinations appear in $h_{\rm eff}$ and are relevant to neutrino oscillations.

In deriving Eq. (14), we have focused on operators of renormalizable dimension, which involve linear derivatives in the equations of motion and a single power of momentum in the Hamiltonian. Operators of nonrenormalizable mass dimension $n>4$ are also of potential importance [3,4]. They appear as higher-derivative terms in the action, along with corresponding complications in the equations of motion and in the construction of the Hamiltonian. An operator of dimension n is associated with a term in the action involving $d=n-3$ derivatives, and the associated terms in the effective Hamiltonian involve d powers of the momentum. The corresponding coefficient for Lorentz violation carries $d+2$ or fewer Lorentz indices, depending on the spinor structure of the coupling and the number of momentum contractions occurring. For the case $n>4$, we generically denote the coefficients by $(k_d)^{\lambda\cdots}$. These coefficients have mass dimension $1-d$. Note that, depending on the theory considered, the mechanism for Lorentz and *CPT* violation can cause them to be suppressed by d-dependent powers of the Planck scale [3,4]. Some effects of operators with $d=2$ have been considered in the context of quantum gravity in Ref. [30].

The mixing described by Eq. (14) or its generalization to operators of dimension $n>4$ can be strongly energy dependent. For example, any nonzero mass-squared differences dominate the Hamiltonian at some low-energy scale. However, while mass effects decrease with energy, Lorentz-violating effects involving operators of renormalizable dimension remain constant or grow linearly with energy E and so always dominate at high energies. For instance, the contributions from a mass of 0.1 eV and a dimensionless coefficient of 10^{-17} are roughly comparable at an energy determined by $E^2\sim(0.1\ \mathrm{eV})^2/(10^{-17})$, or $E\sim 30$ MeV. Below this energy the mass term dominates, while above it the Lorentz-violating term does. Similarly, a dimension-one coefficient of 10^{-15} GeV has a transition energy $E\sim 10$ keV. More generally, effects controlled by the coefficients $(k_d)^{\lambda\cdots}$ for Lorentz violation involving operators of dimension $n=d+3$ grow as E^d.

Although the perturbative diagonalization leading to Eq. (14) is valid for dimensionless coefficients much smaller than one and for energies much greater than any masses or coefficients of dimension one, at sufficiently high energies issues of stability and causality may require the inclusion of Lorentz-violating terms of nonrenormalizable dimension in the theory. In the context of the single-fermion QED extension, for example, a dimensionless c^{00} coefficient can lead to issues with causality and stability at energies $\sim m_{\rm fermion}/\sqrt{c^{00}}$ unless the effects of operators of nonrenormalizable dimension are incorporated [4]. A complete resolution of this issue would be of interest but lies beyond our present scope. It is likely to depend on the underlying mechanisms leading to mass and Lorentz violation, and it may be complicated further by the presence of multiple generations and the sterile neutrino sector. We limit our remarks here to noting that the values of the coefficients for Lorentz violation considered in all the models in this work are sufficiently small that issues of stability and causality can be arranged to appear only beyond experimentally relevant energies. In any case, the renormalizable sector provides a solid foundation for the basic treatment of Lorentz and *CPT* violation in neutrinos.

C. Neutrinos in matter

In many situations, neutrinos traverse a significant volume of ordinary matter before detection. The resulting forward scattering with electrons, protons, and neutrons can have dramatic consequences on neutrino oscillations [51]. These matter interactions can readily be incorporated into our general formalism. Since the effective Lagrangian in normal matter is given by $\Delta\mathcal{L}_{\rm matter}=-\sqrt{2}G_F n_e\overline{\nu_e}\gamma^0 P_L\nu_e+(G_F n_n/\sqrt{2})\overline{\nu_a}\gamma^0 P_L\nu_a$, matter effects are equivalent to contributions from *CPT*-odd coefficients

$$(a_{L,\rm eff})^0_{ee}=G_F(2n_e-n_n)/\sqrt{2},$$

$$(a_{L,\rm eff})^0_{\mu\mu}=(a_{L,\rm eff})^0_{\tau\tau}=-G_F n_n/\sqrt{2}, \tag{18}$$

where n_e and n_n are the number densities of electrons and neutrons. Adding these terms to the effective Hamiltonian (14) therefore incorporates the effects of matter.

For some of the analyses of Lorentz violation below, it is useful to review the treatment of matter effects in solar and

atmospheric neutrinos. Consider first solar neutrinos. These are produced in several processes that generate distinct, well-understood ν_e spectra. The most notable are the pp spectrum with a maximum energy of about 0.4 MeV, and the ^{8}B spectrum with a maximum of about 16 MeV [52]. For $\nu_a \leftrightarrow \nu_b$ mixing scenarios, the contribution from n_n is the same for all species and therefore can be ignored. However, n_n may be important for $\nu_a \leftrightarrow \overline{\nu}_b$ mixing, such as that generated by the coefficients $(g^{\mu\nu\sigma}\mathcal{C})_{ab}$ and $(H^{\mu\nu}\mathcal{C})_{ab}$ in $h_{\rm eff}$. An analytic approximation to the electron number density inside the Sun is given by [52] $n_e/N_A = 245e^{-10.54R/R_\odot}$. It is useful to define $n_s = n_e - \frac{1}{2}n_n$, a combination that often appears in sterile-neutrino searches. This number density has a similar approximation, $n_s/N_A = 223e^{-10.54R/R_\odot}$. The two linearly independent combinations can therefore be taken as $G_F n_e \simeq 1.32\times10^{-20}e^{-10.54R/R_\odot}$ GeV and $G_F n_s \simeq 1.20\times10^{-20}e^{-10.54R/R_\odot}$ GeV, corresponding to a neutron contribution of $G_F n_n = 2G_F(n_e - n_s) \simeq 0.24\times10^{-20}e^{-10.54R/R_\odot}$ GeV to the effective Hamiltonian. These quantities set the scale for matter effects in the Sun.

Next, consider the detection of atmospheric neutrinos. Upward-going neutrinos pass through the Earth and therefore experience higher matter potentials than the downward-going neutrinos, which traverse the less dense atmosphere and a small amount of bedrock on their way to the detector. A crude estimate of the matter potential in this case can be obtained by assuming that the Earth consists of roughly equal numbers of protons, neutrons, and electrons. Using the average number density then yields the approximate value $G_F n_e \simeq G_F n_n \simeq 1.5\times10^{-22}$ GeV. This produces a matter potential similar to that from the Sun at $R/R_\odot \sim 2/5$.

Overall, the contribution to $h_{\rm eff}$ from matter ranges from about 10^{-20} to 10^{-25} GeV. This means that matter effects must be incorporated when the contributions from mass or Lorentz violation lie near these values. This range is comparable to the scale of coefficients for Lorentz violation that originate as suppressed effects from the Planck scale. Note also that most terrestrial experiments involve neutrinos that traverse at least some amount of bedrock or other shielding materials, which can result in substantially different conventional or Lorentz-violating dynamics relative to the vacuum-oscillation case [53].

D. Neutrino oscillations

The analysis of neutrino mixing proceeds along the usual lines. The effective Hamiltonian can be diagonalized with a 6×6 unitary matrix $U_{\rm eff}$:

$$h_{\rm eff} = U_{\rm eff}^\dagger E_{\rm eff} U_{\rm eff}, \tag{19}$$

where $E_{\rm eff}$ is a 6×6 diagonal matrix. In contrast to the Lorentz-covariant case, where mixing without sterile neutrinos involves only three propagating states, here mixing without sterile neutrinos may occur with six states. This means that there can be up to five energy-dependent eigenvalue differences for Lorentz-violating mixing, resulting in five independent oscillation lengths instead of the usual two [54].

Denoting the six propagation states by the amplitudes $B_J(t;\vec{p})$ with $J=1,\ldots,6$, we can write $B_J(t;\vec{p}) = \tilde{U}_{Ja}b_a(t;\vec{p}) + \overline{U}_{Ja}d_a(t;\vec{p})$, where we have split $U_{\rm eff}$ into 6×3 matrices $U_{\rm eff} = (\tilde{U},\overline{U})$. The time evolution operator may then be written as

$$\begin{aligned} S_{ab}(t) &= (U_{\rm eff}^\dagger e^{-iE_{\rm eff}t}U_{\rm eff})_{ab} \\ &= \begin{pmatrix} S_{\nu_a\nu_b}(t) & S_{\nu_a\overline{\nu}_b}(t) \\ S_{\overline{\nu}_a\nu_b}(t) & S_{\overline{\nu}_a\overline{\nu}_b}(t) \end{pmatrix} \\ &= \sum_J e^{-itE_{(J)}} \begin{pmatrix} \tilde{U}_{Ja}^*\tilde{U}_{Jb} & \tilde{U}_{Ja}^*\overline{U}_{Jb} \\ \overline{U}_{Ja}^*\tilde{U}_{Jb} & \overline{U}_{Ja}^*\overline{U}_{Jb} \end{pmatrix}, \end{aligned} \tag{20}$$

where $E_{(J)}$ are the diagonal values of $E_{\rm eff}$.

The probabilities for a neutrino of type b oscillating into a neutrino or antineutrino of type a in time t are therefore $P_{\nu_b\to\nu_a}(t) = |S_{\nu_a\nu_b}(t)|^2$ or $P_{\nu_b\to\overline{\nu}_a}(t) = |S_{\overline{\nu}_a\nu_b}(t)|^2$, respectively. Similarly, for antineutrinos we have $P_{\overline{\nu}_b\to\nu_a}(t) = |S_{\nu_a\overline{\nu}_b}(t)|^2$ or $P_{\overline{\nu}_b\to\overline{\nu}_a}(t) = |S_{\overline{\nu}_a\overline{\nu}_b}(t)|^2$. In terms of the matrices $\tilde{U}$ and $\overline{U}$, the probabilities are

$$P_{\nu_b\to\nu_a}(t) = \delta_{ab} - 4\sum_{J>K} \mathrm{Re}(\tilde{U}_{Ja}^*\tilde{U}_{Jb}\tilde{U}_{Ka}\tilde{U}_{Kb}^*)\sin^2\frac{\Delta_{JK}t}{2} + 2\sum_{J>K} \mathrm{Im}(\tilde{U}_{Ja}^*\tilde{U}_{Jb}\tilde{U}_{Ka}\tilde{U}_{Kb}^*)\sin\Delta_{JK}t, \tag{21a}$$

$$P_{\overline{\nu}_b\to\overline{\nu}_a}(t) = \delta_{ab} - 4\sum_{J>K} \mathrm{Re}(\overline{U}_{Ja}^*\overline{U}_{Jb}\overline{U}_{Ka}\overline{U}_{Kb}^*)\sin^2\frac{\Delta_{JK}t}{2} + 2\sum_{J>K} \mathrm{Im}(\overline{U}_{Ja}^*\overline{U}_{Jb}\overline{U}_{Ka}\overline{U}_{Kb}^*)\sin\Delta_{JK}t, \tag{21b}$$

$$P_{\nu_b\to\overline{\nu}_a}(t) = -4\sum_{J>K} \mathrm{Re}(\overline{U}_{Ja}^*\tilde{U}_{Jb}\overline{U}_{Ka}\tilde{U}_{Kb}^*)\sin^2\frac{\Delta_{JK}t}{2} + 2\sum_{J>K} \mathrm{Im}(\overline{U}_{Ja}^*\tilde{U}_{Jb}\overline{U}_{Ka}\tilde{U}_{Kb}^*)\sin\Delta_{JK}t, \tag{21c}$$

$$P_{\overline{\nu}_b\to\nu_a}(t) = -4\sum_{J>K} \mathrm{Re}(\tilde{U}_{Ja}^*\overline{U}_{Jb}\tilde{U}_{Ka}\overline{U}_{Kb}^*)\sin^2\frac{\Delta_{JK}t}{2} + 2\sum_{J>K} \mathrm{Im}(\tilde{U}_{Ja}^*\overline{U}_{Jb}\tilde{U}_{Ka}\overline{U}_{Kb}^*)\sin\Delta_{JK}t, \tag{21d}$$

where the effective-energy difference is denoted by $\Delta_{JK} = E_{(J)} - E_{(K)}$.

E. *CPT* properties

With a conveniently chosen phase, *CPT* may be implemented by the transformation

$$\begin{pmatrix} b_a^{CPT}(t;\vec{p}) \\ d_a^{CPT}(t;\vec{p}) \end{pmatrix} = i \begin{pmatrix} -d_a^*(-t;\vec{p}) \\ b_a^*(-t;\vec{p}) \end{pmatrix} \equiv \sigma^2 \begin{pmatrix} b_a^*(-t;\vec{p}) \\ d_a^*(-t;\vec{p}) \end{pmatrix}. \tag{22}$$

This yields precisely the expected result when applied to $h_{\rm eff}$: the *CPT*-conjugate Hamiltonian $h_{\rm eff}^{CPT} = \sigma^2 h_{\rm eff}^* \sigma^2$ can be obtained from Eq. (14) by changing the sign of the *CPT*-odd a_L and g coefficients. Then, $h_{\rm eff}^{CPT} = h_{\rm eff}$ when a_L and g vanish, as expected. A notable feature here is that independent mass matrices for neutrinos and antineutrinos cannot be generated as has been proposed [55]. Greenberg has recently proved that this result is general [5].

Under CPT, the transition amplitudes transform as

$$S_{\nu_a \nu_b}(t) \overset{CPT}{\leftrightarrow} S^*_{\bar{\nu}_a \bar{\nu}_b}(-t), \tag{23a}$$

$$S_{\bar{\nu}_a \nu_b}(t) \overset{CPT}{\leftrightarrow} -S^*_{\nu_a \bar{\nu}_b}(-t). \tag{23b}$$

These relations become equalities if CPT holds. The first relation then yields the usual result

$$CPT \text{ invariance} \Rightarrow P_{\nu_b \to \nu_a}(t) = P_{\bar{\nu}_a \to \bar{\nu}_b}(t). \tag{24a}$$

This property has long been understood and has been identified as a potential test of *CPT* invariance [25]. However, the negation of terms in this result produces a statement that may be false in general because *CPT* violation need not imply $P_{\nu_b \to \nu_a}(t) \neq P_{\bar{\nu}_a \to \bar{\nu}_b}(t)$. Examples of models that violate *CPT* but nonetheless satisfy Eq. (24a) are given in Sec. IV.

The above property addresses the relationship between $\nu \leftrightarrow \nu$ and $\bar{\nu} \leftrightarrow \bar{\nu}$ mixing. There is also an analogous property associated with $\nu \leftrightarrow \bar{\nu}$ mixing. Thus, for *CPT* invariance, relation (23b) yields the additional result

$$CPT \text{ invariance} \Rightarrow P_{\nu_b \rightleftarrows \bar{\nu}_a}(t) = P_{\nu_a \rightleftarrows \bar{\nu}_b}(t). \tag{24b}$$

This property may also provide opportunities to test for Lorentz and *CPT* invariance. Note, however, that negation of its terms produces a statement that may be false in general, as in the previous case.

Finally, we emphasize that the presence of *CPT* violation increases the number of independent oscillation lengths without the addition of sterile neutrinos. In the general case, nonzero coefficients for *CPT* violation in the effective Hamiltonian (14) can generate up to six independent propagating states, rather than the usual three.

F. Reference frames

The presence of Lorentz violation makes it necessary to specify the frame in which experimental results are reported. Coordinate invariance of the physics, in particular observer Lorentz invariance [2], ensures that the analysis and measurements of an experiment can be performed in any frame of reference. However, it is convenient to have a standard set of frames to facilitate comparisons of different experiments. In the literature, measurements are conventionally expressed in terms of coefficients for Lorentz violation defined in a Sun-centered celestial equatorial frame with coordinates (T,X,Y,Z) [56]. For our present purposes, it suffices to identify the Z direction as lying along the Earth's rotational axis and the X direction as pointing towards the vernal equinox. The coefficients for Lorentz violation in any other inertial frame can be related to the standard set in the Sun-centered frame by an observer Lorentz transformation. In general, this transformation includes both rotations and boosts, but boost effects are frequently neglected because they introduce only terms suppressed by the velocity β between frames, which is typically $\lesssim 10^{-4}$. Recently, studies of some β-suppressed terms have been performed in the context of high-precision clock-comparison experiments [15,16] and resonant cavities [21,22].

The existence of orientation-dependent effects makes it useful to define a standard parametrization for the direction of neutrino propagation $\hat{p}$ and the corresponding $\hat{\epsilon}_1, \hat{\epsilon}_2$ vectors in the Sun-centered frame. A suitable set of unit vectors is given by

$$\begin{aligned} \hat{p} &= (\sin\Theta\cos\Phi, \sin\Theta\sin\Phi, \cos\Theta), \\ \hat{\epsilon}_1 &= (\cos\Theta\cos\Phi, \cos\Theta\sin\Phi, -\sin\Theta), \\ \hat{\epsilon}_2 &= (-\sin\Phi, \cos\Phi, 0), \end{aligned} \tag{25}$$

where Θ and Φ are the celestial colatitude and longitude of propagation, respectively. We remark that these quantities are related to the right ascension r and declination d of the source as viewed from the detector by $\Theta = 90° + d$ and $\Phi = 180° + r$.

In the remainder of this subsection, we provide some technical comments about the frame dependence of our choice of spinor basis in Sec. II B. This basis is normally associated with massless fermions, so the presence of mass or Lorentz violation means that even with a covariant normalization the corresponding amplitudes are no longer scalar functions under observer Lorentz transformations and hence are frame dependent. However, our basis suffices for perturbative calculations in which the physically significant states are affected only by masses and coefficients for Lorentz violation that are small relative to $|\vec{p}|$, while the complexity of the general Lorentz-violating case makes the decomposition into a covariant basis impractical. Moreover, despite the frame-dependent nature of the calculation, the probabilities (21) are frame independent at leading order. In the usual case, frame independence follows from the Lorentz-vector nature of the exact four-momenta $(E_{(J)};\vec{p})$, which implies the products $E_{(J)}t - \vec{p}\cdot\vec{x}$ are Lorentz scalars, and from the constancy and frame-independence of the mixing matrix $U_{\rm eff}$. It turns out that a version of these properties holds in the present case, as we show next.

First, we observe that the elements of the 6×6 matrix $|\vec{p}|(h_{\rm eff}-|\vec{p}|)$ are scalars under observer Lorentz transformations at leading order in small quantities. Next, note that the matrix $U_{\rm eff}$ diagonalizes $|\vec{p}|(h_{\rm eff}-|\vec{p}|)$, so its elements can be chosen to be observer Lorentz scalars as well. In turn, this means that the diagonal elements $|\vec{p}|(E_{(J)}-|\vec{p}|)$ are also observer Lorentz scalars, since they are functions of the elements of $|\vec{p}|(h_{\rm eff}-|\vec{p}|)$. From this result, it follows explicitly that the neutrino dispersion relations $E_{(J)}^2-\vec{p}^{\,2}$ are observer Lorentz scalars at leading order, since

$$E_{(J)}^2-\vec{p}^{\,2}=(E_{(J)}+|\vec{p}|)(E_{(J)}-|\vec{p}|)$$
$$\simeq 2|\vec{p}|(E_{(J)}-|\vec{p}|). \tag{26}$$

The four-momentum is therefore a vector under observer Lorentz transformations to leading order, as desired. Combining this property with the scalar character of $U_{\rm eff}$ implies that the leading-order transition amplitudes and probabilities (21) are covariant under observer Lorentz transformations, as claimed.

III. SENSITIVITIES

A. Existing constraints

To date, there is no compelling experimental evidence for nonzero coefficients for Lorentz violation in any sector. Theoretical predictions of the size of the effects depend on the underlying model. However, the natural scale for a fundamental theory is the Planck mass m_P, which is about 17 orders of magnitude greater than the electroweak scale m_W relevant to the SM and roughly 30 orders of magnitude greater than the scale of neutrino masses, if they exist. It is plausible that any observable Lorentz- and *CPT*-violating effects are suppressed by one or more powers of the dimensionless ratio $r=m/m_P\lesssim10^{-17}$, where m is the relevant low-energy scale and m_P is the Planck mass [7]. In contrast, the scale of observed neutrino oscillations is $\lesssim0.1$ eV, which enters as a squared mass $\Delta m^2\lesssim10^{-20}$ GeV. At physically relevant energies, 10^{-4} GeV$<E<10^3$ GeV, the oscillation physics is determined by the dimensionless ratio $r_\nu=\Delta m^2/E^2$. Remarkably, the two dimensionless ratios r and r_ν have a similar range, so the natural size of Lorentz- and *CPT*-violating effects may be comparable to the natural size of neutrino-oscillation effects.

Certain experiments in the fermion and photon sectors have achieved sensitivities corresponding to dimensionless suppressions of roughly 10^{-30}. Since the coefficients for Lorentz violation in the various sectors can be related either directly through symmetries or indirectly through radiative corrections, it might seem that existing experimental constraints severely restrict the possibilities for Lorentz violation in neutrinos. In fact, this expectation is incorrect, as we discuss next.

In the context of $h_{\rm eff}$, the relevant coefficients are $(a_L)_{ab}^{\mu}$ and $(c_L)_{ab}^{\mu\nu}$, since these appear directly in the charged-fermion sector of the SME. A decomposition of the multiflavor QED limit of the charged-lepton sector can be performed in analogy with Eq. (2). It produces the identification

$$a_{ab}^{\mu}=\frac{1}{2}(a_L+a_R)_{ab}^{\mu},$$
$$b_{ab}^{\mu}=\frac{1}{2}(a_L-a_R)_{ab}^{\mu},$$
$$c_{ab}^{\mu\nu}=\frac{1}{2}(c_L+c_R)_{ab}^{\mu\nu},$$
$$d_{ab}^{\mu\nu}=\frac{1}{2}(c_L-c_R)_{ab}^{\mu\nu}, \tag{27}$$

where $(c_R)_{ab}^{\mu\nu}$ and $(a_R)_{ab}^{\mu}$ are coefficients in the SME that couple to right-handed leptons and therefore leave unaffected the active neutrinos at tree level. On this basis, it might naively appear that the charged sector is sensitive to more combinations of coefficients for Lorentz violation than the neutrino sector. However, the mass hierarchy of the charged leptons e,μ,τ implies that only coefficients that are diagonal in flavor space appear in leading-order perturbative calculations. As a result, e,μ,τ effectively decouple, resulting in three independent copies of the fermion sector in the Lorentz- and *CPT*-violating QED extension. This implies that unsuppressed sensitivity to Lorentz violation in the charged-lepton sector involves only flavor-diagonal components. Moreover, the decoupling also implies that certain coefficients such as $a_{ee}^{\mu},a_{\mu\mu}^{\mu},a_{\tau\tau}^{\mu}$ are physically unobservable, further reducing the total number of coefficients affecting charged leptons. Taken together, these factors ensure that the *CPT*-odd sectors of charged leptons and neutrinos are completely independent at tree level. Similar arguments apply to parts of the *CPT*-even sector as well. We therefore conclude that neutrinos are sensitive to a greater number of coefficients for Lorentz violation than the charged leptons, and at tree level most of these coefficients are independent from those accessible with e, μ, or τ leptons.

Particularly stringent constraints exist on some components of the charged-lepton coefficients b_{ee}^{μ} and $b_{\mu\mu}^{\mu}$. Although these are linearly independent of neutrino-sector coefficients at tree level, it is natural to ask whether radiative corrections to these components can be used to constrain possible neutrino effects. As an example, Ref. [28] explores the possibility that eV-size effects in heavy sterile neutrinos could evade the constraints in the charged-lepton sector, finding that within a standard seesaw mechanism the existence of large b^{μ}-type coefficients for sterile neutrinos tends to produce b^{μ} coefficients in the charged-lepton sector that conflict with observation. In this work, we neglect seesaw-induced coefficients because they are suppressed by the large-mass scale. However, it is of interest to ask whether radiative corrections alter the tree-level independence of the charged- and neutral-lepton sectors.

For simplicity, we restrict our discussion to the relevant a^{μ} and b^{μ} coefficients, although related remarks apply also to $c^{\mu\nu}$ and $d^{\mu\nu}$ coefficients. The leading-order radiative cor-

rections are linear in the coefficients for Lorentz violation. However, loops involving weak interactions are heavily suppressed by additional factors at the relevant energies, while strong interactions play no role. We can therefore restrict attention to the QED extension. In this case, general properties of the coefficients for Lorentz violation under the discrete symmetries C, P, and T imply that corrections to b^μ coefficients involve only other b^μ type coefficients [57]. As a result, although the constraints from charged-lepton experiments may restrict b^μ in the neutrino sector of the SME, the a^μ coefficients are unaffected and so a_L is unconstrained. Thus, the independence of the charged- and neutral-lepton sectors remains valid for radiative corrections.

B. General features

In the presence of Lorentz and *CPT* violation, a wide range of unconventional neutrino behaviors can occur. These include unusual energy dependence, direction-dependent effects, and neutrino-antineutrino mixing. Specific examples of these behaviors are illustrated in the examples presented in Sec. IV. Here, we focus on some general features of experimental sensitivities to Lorentz- and *CPT*-violating effects. Some of these have been discussed in the context of the minimal SME in our earlier work [29], but the present discussion holds for the full theory (14) and generically for operators of nonrenormalizable dimension.

Figure 1 shows an estimate of the coverage in baseline distance L versus energy E of the currently published neutrino-oscillation data. Included in the evidence for oscillations are observations of solar neutrinos by Cl- and Ga-based experiments [37–40], Super Kamiokande (SK) [41], and SNO [42]; and of atmospheric neutrinos by SK [36], reactor-based KamLAND [43], and accelerator-based LSND [44] and K2K [45]. Null results include the reactor experiments Bugey [58], CHOOZ [59], Gösgen [60], Palo Verde [61], and various accelerator-based short-baseline experiments including, for example, the high-energy experiments BNL-E776 [62], CCFR [63], CHORUS [64], NOMAD [65,66], NuTeV [67], and the low-energy KARMEN [68]. A number of new accelerator-based experiments are likely to produce interesting results in the near future. These include the short-baseline ($L \simeq 500$ m, $E \simeq 1$ GeV) MiniBooNE experiment [69] designed to test the LSND anomaly, and the long-baseline ($L \simeq 700$ km, $E \simeq 1$ GeV) ICARUS [70], MINOS [71], and OPERA [72] experiments, which are planned to test the atmospheric-oscillation hypothesis. Also shown on the figure are the approximate effective regions associated with the matter potentials for the Sun and the Earth.

The unusual energy dependence can be viewed as a consequence of the dimensionality of the coefficients for Lorentz violation. The standard scenario for neutrino oscillations involves mass-squared differences Δm^2 that combine with the baseline distance L and the neutrino energy E to yield the physically relevant dimensionless combination $\Delta m^2 L/E$. However, Eq. (14) shows that Lorentz-violating oscillations generated by the dimension-one coefficients $a^\mu, b^\mu, H^{\mu\nu}$ are controlled by the dimensionless combinations

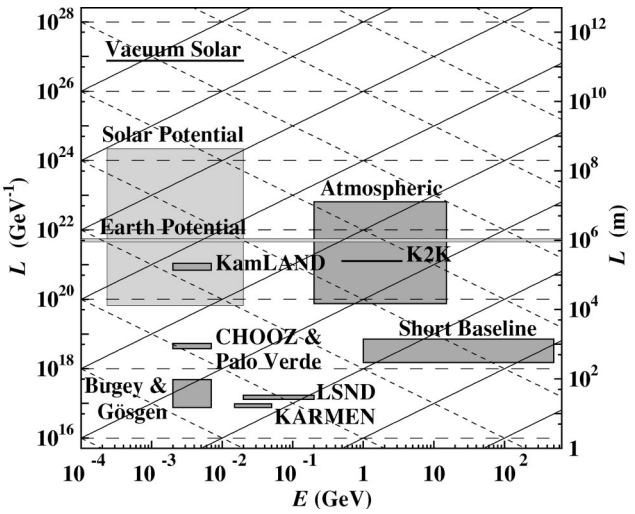

FIG. 1. Approximate sensitivities of various experiments. Lines of constant L/E (solid), L (dashed), and LE (dotted) are shown, giving approximate sensitivities to the quantities $\{m, m_5\}$, $\{a^\mu, b^\mu, H^{\mu\nu}\}$, and $\{c^{\mu\nu}, d^{\mu\nu}, g^{\mu\nu\sigma}\}$, respectively. Also shown are the approximate effective regions for the matter potential in the Sun and Earth.

$a^\mu L$, $b^\mu L$, $H^{\mu\nu} L$, while those generated by $c^{\mu\nu}$, $d^{\mu\nu}$, $g^{\mu\nu\sigma}$ are controlled by $c^{\mu\nu} LE$, $d^{\mu\nu} LE$, $g^{\mu\nu\sigma} LE$. More generally, oscillations generated by a coefficient $(k_d)^{\lambda\cdots}$ for a Lorentz-violating operator of nonrenormalizable dimension $n = d + 3$ are controlled by $(k_d)^{\lambda\cdots} LE^d$.

Figure 1 illustrates these various energy dependences. Lines of constant L/E, L, and LE are plotted, bounding approximate regions of experimental sensitivity to conventional mass-squared differences, dimension-one coefficients, and dimensionless coefficients, respectively. For each nonzero coefficient in h_{eff}, a bounding line on this figure exists above which the corresponding Lorentz-violating effects become of order one. Given such a line, any experiments located near or above it can be affected by the associated coefficient, but experiments below it have limited or no sensitivity. For example, the region of limiting sensitivity for a hypothetical dimensionless coefficient of magnitude $\sim 10^{-18}$ is bounded approximately by the dimensionless line satisfying $LE = 10^{18}$, which is the dotted line running just below KamLAND. Experiments lying above this line, such as KamLAND, SNO, and SK, could be sensitive to the effects of this coefficient. Note that approximate regions of experimental sensitivity to coefficients $(k_d)^{\lambda\cdots}$ of dimension $1-d$ could also be identified on the figure. They would be bounded by lines of constant LE^d with $d > 1$, which have negative-integer slopes.

Figure 1 also reveals that experiments and data allow probes well below the 10^{-17} Planck-suppression level. For instance, the various null results from short-baseline reactor and accelerator experiments could be reanalyzed to yield upper bounds on certain coefficients for Lorentz violation. Thus, the high-energy experiments CHORUS and NOMAD found no evidence of $\nu_{e,\mu} \to \nu_\tau$ at energies $E \sim 100$ GeV and at distances $L \sim 10^{18}$ GeV^{-1}, which suggests that reanalyzes of these experiments would yield interesting new sensitivi-

ties of roughly 10^{-18} GeV to dimension-one coefficients and roughly 10^{-20} to dimensionless coefficients. A similar situation holds for low-energy experiments such as CHOOZ, Palo Verde, and KARMEN in the $\bar{\nu}_e$ sector. From Fig. 1 we see that, relative to CHORUS and NOMAD, CHOOZ and Palo Verde might be expected to have comparable sensitivities to dimension-one coefficients but reduced sensitivity to dimensionless ones, while KARMEN has comparable sensitivity to conventional mass effects. In each case, the attainable sensitivities also depend on various experiment-dependent factors, so individual reanalyzes are required to make definitive statements.

Another unusual effect due to Lorentz violation is direction-dependent neutrino behavior, a consequence of rotation-symmetry violation. This has consequences for comparisons of results between different terrestrial experiments or for the analysis of experiments involving multiple sources, since the orientation of the neutrino beam or the location of the source relative to the detector can affect neutrino oscillations. Rotation-symmetry violation also implies that the daily rotation of the Earth about its axis induces apparent periodic changes of the coefficients for Lorentz violation in the laboratory, which would be manifest as temporal variations in neutrino oscillations. These variations occur at multiples of the sidereal frequency $\omega_\oplus \simeq 2\pi/(23\ \mathrm{h}\ 56\ \mathrm{min})$. Similarly, in the presence of rotation-symmetry violation, neutrinos emitted from the Sun in different directions undergo different oscillations, which may produce observable annual variations arising from the change in the location of the detector as the Earth orbits the Sun. All these temporal variations with appropriate periodicity provide unique signals of Lorentz violation in neutrino oscillations. Moreover, they can also yield interesting sensitivities to certain coefficients. For instance, SK found that the shape of the solar-neutrino flux matches the expected value to within about 5% over the year [41]. The Sun-Earth distance is $L \sim 10^{27}\ \mathrm{GeV}^{-1}$, and $LE \sim 10^{25}$ for the SK energy range, so a reanalysis of the SK data might achieve impressive sensitivities of $\sim 10^{-28}$ GeV to dimension-one coefficients and $\sim 10^{-26}$ to dimensionless ones, comparable to the best experimental sensitivities achieved for other sectors of the SME.

Another interesting feature of Lorentz violation involves novel resonance effects in neutrino oscillations. In the conventional case with neutrino masses, the usual MSW resonances [35] arise when the local matter environment is such that neutrino interactions become comparable to mass effects, thereby drastically changing the character of the Hamiltonian. The presence of Lorentz violation can trigger several other types of effects, including resonances without mass or matter that involve different coefficients for Lorentz violation, resonances involving coefficients for Lorentz violation and mass terms, resonances involving coefficients for Lorentz violation and matter effects, and various combinations of the above. The earliest example of an explicit vacuum resonance in a two-generation model involving a mass term and a single nonzero coefficient $(a_L)^T$ for Lorentz and *CPT* violation is given in Ref. [25]. An example of a vacuum resonance in a three-generation model involving two coefficients $(a_L)^Z$ and $(c_L)^{TT}$ for Lorentz and *CPT* violation occurs in the bicycle model of Ref. [29]. We emphasize that resonances due to Lorentz violation can occur in the vacuum as well as in matter, and not only at particular energies but also for particular directions of propagation. Note also that, even away from the resonance regions, matter effects may be important when considering mass terms or coefficients for Lorentz violation that have lines of sensitivity near or above the Sun- or Earth-potential regions shown in Fig. 1.

C. The LSND anomaly

In the LSND experiment [44], copious numbers of neutrinos were produced from the decay of π^+ at rest. This process is dominated by the decay $\pi^+ \to \mu^+ \nu_\mu$ followed by $\mu^+ \to e^+ \nu_e \bar{\nu}_\mu$. A small excess in $\bar{\nu}_e$ was seen, interpreted as the oscillation $\bar{\nu}_\mu \to \bar{\nu}_e$ with a small probability of about 0.26%. This result is difficult to accommodate within the context of the conventional global analysis [31], in which two mass-squared differences are used to describe solar and atmospheric oscillation data. The solar data appear consistent with a mass-squared difference $\delta m^2 \sim 10^{-5}\ \mathrm{eV}^2$, while the atmospheric data suggest a second mass-squared difference $\Delta m^2 \sim 10^{-3}\ \mathrm{eV}^2$. The regions of limiting sensitivity to these mass-squared differences are shown in Fig. 1, where lines of constant L/E with values $L/E \sim 10^{23}\ \mathrm{GeV}^{-2}$ and $L/E \sim 10^{21}\ \mathrm{GeV}^{-2}$ can be seen. Experiments lying significantly below these lines, including LSND, should be insensitive to oscillations caused by δm^2 and Δm^2. This illustrates the difficulty in explaining the LSND result within the conventional framework without introducing additional mass-squared differences.

A resolution of this LSND anomaly without the introduction of sterile neutrinos might emerge from the unusual energy dependence, the directional dependence, or the neutrino-antineutrino mixing introduced by Lorentz violation. For example, equal numbers of $\bar{\nu}_\mu$, ν_e, and $\bar{\nu}_\mu$ are produced in LSND, so if ν_e mix with $\bar{\nu}_e$ then the observed excess in $\bar{\nu}_e$ may be a result of $\nu_e \leftrightarrow \bar{\nu}_e$ mixing rather than $\bar{\nu}_\mu \leftrightarrow \bar{\nu}_e$ mixing. We note, however, that if the possible direction dependence is neglected then Fig. 1 shows that a simple solution based either on the unusual energy dependence or on $\nu \leftrightarrow \bar{\nu}$ mixing is likely to be hindered by existing null results in the $\bar{\nu}_e$ sector, from low-energy experiments such as CHOOZ and Palo Verde or from high-energy experiments such as CHORUS, NOMAD, and NuTeV. Indeed, from this figure we see generically that to explain the LSND result one needs a mass-squared difference of about $10^{-19}\ \mathrm{GeV}^2 = 10^{-1}\ \mathrm{eV}^2$, a dimension-one coefficient of about 10^{-18} GeV or a dimensionless coefficient of about 10^{-17}. Note that each of these has consequences for other experiments, depending on flavor content. For example, the upcoming MiniBooNE experiment is designed to test the same oscillation channel and will therefore be sensitive to all three possibilities.

IV. ILLUSTRATIVE MODELS

To illustrate some of the novel behaviors of neutrino oscillations in the presence of Lorentz and *CPT* violation, we next consider a number of simple special cases of the theory (14) with only one or a few nonzero coefficients. For each case, some of the ways that the unusual neutrino behaviors might affect current observations are quantitatively examined. Also, we simplify expressions by adopting temporary notation for the specific nonzero coefficients for Lorentz violation within each model: quantities carrying a ring accent, such as $\mathring{c}$, denote rotation-symmetric coefficients; while those with a háček accent, such as $\check{c}$, denote anisotropic coefficients.

A. Rotationally invariant models

The rotation-invariant restriction provides an interesting special limit of the theory (14). While difficult to motivate without knowledge of the underlying mechanism leading to Lorentz and *CPT* violation, rotation invariant or so-called ''fried-chicken'' (FC) models are attractive because rotation symmetry can significantly reduce the complexity of calculations, thereby providing a simple context within which to study the unusual neutrino behaviors arising from Lorentz violation.

Restricting $h_{\rm eff}$ to FC terms leaves only four matrices, $(\widetilde{m}^2)_{ab}$, $(a_L)^0_{ab}$, $(c_L)^{00}_{ab}$, and $(c_L)^{jk}_{ab}=\frac{1}{3}(c_L)^{ll}_{ab}\delta^{jk}$. As described in Sec. II B, the trace $(c_L)^{00}_{ab}-(c_L)^{jj}_{ab}$ is unobservable and may be set to zero, so only three of these matrices are independent. Dropping the irrelevant kinetic term and assuming rotation invariance in the Sun-centered (T,X,Y,Z) frame for definiteness, the 6×6 effective Hamiltonian reduces to the block-diagonal form

$$(h_{\rm eff})^{\rm FC}_{ab}={\rm diag}\left\{\left[\widetilde{m}^2/(2E)+(a_L)^T-\frac{4}{3}(c_L)^{TT}E\right]_{ab},\right.$$
$$\left.\left[\widetilde{m}^2/(2E)-(a_L)^T-\frac{4}{3}(c_L)^{TT}E\right]^*_{ab}\right\}. \qquad (28)$$

This Hamiltonian provides a general FC model of three active neutrinos. The generalization to additional light or massless sterile neutrinos is straightforward.

With the exception of the original proposal for Lorentz violation in neutrinos [2] and the recent work in Ref. [29], which address both rotation-invariant and anisotropic effects with and without *CPT* violation, existing works on the subject [24–27] involve limited special cases of the general FC model (28). The bulk of the literature restricts attention to the two-generation special case and neglects either the $(a_L)^T$ term or the $(c_L)^{TT}$ term. A plethora of unexplored models and effects exists.

It might seem logical to impose spherical symmetry in a special frame such as the cosmic microwave background (CMB) frame. However, if rotation symmetry is assumed in the CMB frame then the coefficients in Eq. (28) differ from $(a_L)^T$,$(c_L)^{TT}$ in the standard Sun-centered frame, being instead $(a_L)^0$,$(c_L)^{00}$ in the CMB frame. Relating the latter to the standard Sun-centered frame or any other experimentally attainable frame introduces direction dependence due to the motion of our solar system in the CMB frame. The relevant Hamiltonian then also involves spatial components of the coefficients, so it differs from Eq. (28) and is instead an anisotropic limit of the theory (14).

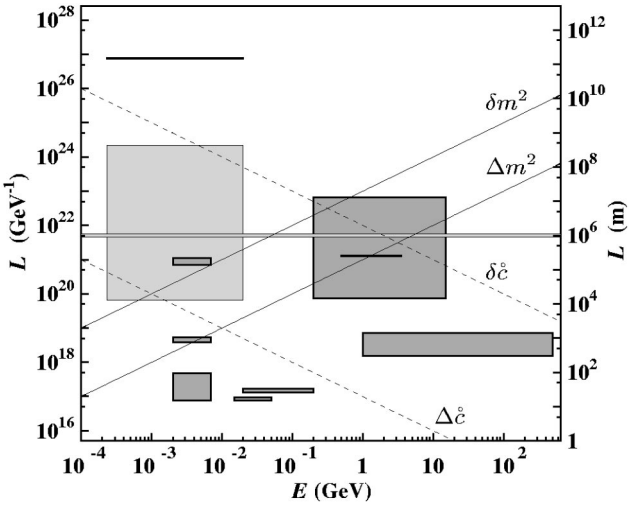

FIG. 2. Lines of limiting sensitivity for $\delta m^2\sim10^{-5}$ eV^2, $\Delta m^2\sim10^{-3}$ eV^2, $\delta\mathring{c}\sim10^{-22}$, $\Delta\mathring{c}\sim10^{-17}$. The shaded regions are those of Fig. 1.

Although the FC model (28) is rather limited considering the wealth of possible effects contained in the full theory (14), and although it has little theoretical motivation other than calculational convenience, further study of this model is useful because it provides a readily workable context within which to gain insight about possible signals of Lorentz and *CPT* violation. This is illustrated in the few simple examples discussed in this subsection.

1. Example: $(c_L)^{TT}_{ab}\neq0$

A particularly simple FC model consists of a single nonzero coefficient matrix such as $(c_L)^{TT}_{ab}$. Some features of this model are similar to the conventional massive-neutrino case, but there is unusual energy dependence. Here, we take advantage of this energy dependence to illustrate one type of mechanism through which Lorentz violation might provide a solution to the LSND anomaly.

Lines of limiting sensitivity for the two mass-squared differences δm^2 and Δm^2 used in the conventional global analysis are shown in Fig. 2. The mixing angles are such that ν_e oscillations are almost completely controlled by δm^2. Therefore, one can expect to see only $\overline{\nu}_e$ mixing in KamLAND, in solar neutrino experiments, and possibly in the lowest-energy atmospheric-neutrino experiments. The observed atmospheric oscillations are due to Δm^2, which controls $\nu_\mu\leftrightarrow\nu_\tau$ mixing. Since LSND lies well below both the δm^2 and the Δm^2 lines, no oscillations are predicted.

Replacing the mass-squared differences δm^2 and Δm^2 with a nonzero coefficient matrix $(c_L)^{TT}_{ab}$ produces an effective Hamiltonian $h_{\rm eff}$ that can be parametrized as described in Appendix B, using two eigenvalue differences and CKM-like mixing angles and phases. For simplicity, we choose here to

mimic the usual solution by taking vanishing phases and θ_{13}^{TT}, and we consider only the case $\theta_{23}^{TT}=\pi/4$. This leaves three degrees of freedom: two eigenvalue differences, and one mixing angle $\theta_{12}^{TT}\equiv\theta$. It turns out to be convenient to work with two linear combinations of the eigenvalue differences, defined by

$$\delta\mathring{c}\equiv\frac{4}{3}[(c_L)_{(3)}^{TT}-(c_L)_{(2)}^{TT}],$$

$$\Delta\mathring{c}\equiv\frac{4}{3}[(c_L)_{(2)}^{TT}-(c_L)_{(1)}^{TT}]. \tag{29}$$

The probabilities for this case are then

$$\begin{aligned}
P_{\nu_e\to\nu_e}&=1-\sin^2 2\theta\sin^2(\Delta\mathring{c}LE/2),\\
P_{\nu_\mu\to\nu_\mu}&=P_{\nu_\tau\to\nu_\tau}=1-\frac{1}{4}\sin^2 2\theta\sin^2(\Delta\mathring{c}LE/2)\\
&\quad-\sin^2\theta\sin^2[(\Delta\mathring{c}+\delta\mathring{c})LE/2]\\
&\quad-\cos^2\theta\sin^2(\delta\mathring{c}LE/2),\\
P_{\nu_e\leftrightarrow\nu_\mu}&=P_{\nu_e\leftrightarrow\nu_\tau}=\frac{1}{2}\sin^2 2\theta\sin^2(\Delta\mathring{c}LE/2),\\
P_{\nu_\mu\leftrightarrow\nu_\tau}&=-\frac{1}{4}\sin^2 2\theta\sin^2(\Delta\mathring{c}LE/2)\\
&\quad+\sin^2\theta\sin^2[(\Delta\mathring{c}+\delta\mathring{c})LE/2]\\
&\quad+\cos^2\theta\sin^2(\delta\mathring{c}LE/2).
\end{aligned} \tag{30}$$

The corresponding antineutrino expressions are identical.

A possible approach is illustrated in the figure. The line of sensitivity for the larger difference $\Delta\mathring{c}$ can be chosen to lie just above CHOOZ and LSND. This produces only a small effect in these experiments and may provide an explanation for LSND that may not conflict with CHOOZ. The remaining difference $\delta\mathring{c}$ can then be chosen to explain atmospheric data. The above situation somewhat resembles the conventional mass solution, with the role of $\delta m^2/2E$ replaced by $\Delta\mathring{c}E$ and that of $\Delta m^2/2E$ replaced by $\delta\mathring{c}E$. The angle θ is the analogue of the solar-neutrino mixing angle. However, the energy dependences of the two cases differ substantially, as is also evident from the figure.

To explore quantitatively how this approach might work, consider the positive LSND and KamLAND results. KamLAND detects $\overline{\nu}_e$ from distant reactors and found about a 61% reduction in the flux. Most reactors are 138–214 km from the detector, and the corresponding $\overline{\nu}_e$ energies fall in the range 1 MeV$\lesssim E\lesssim$10 MeV. If KamLAND lies well above the $\Delta\mathring{c}$ line, the relevant quantity is the average survival probability $\langle P_{\overline{\nu}_e\to\overline{\nu}_e}\rangle=1-\frac{1}{2}\sin^2 2\theta\simeq 61\%$, yielding a mixing angle given by $\sin^2 2\theta\simeq 0.78$. Also, assuming LSND is in a region of small oscillation effects, then we can approximate $P_{\overline{\nu}_\mu\to\overline{\nu}_e}\approx\frac{1}{2}\sin^2 2\theta(\Delta\mathring{c}LE/2)^2\simeq 0.26\%$. Then, for $E\simeq 45$ MeV and $L\simeq 30$ m we obtain $\Delta\mathring{c}\simeq 2.4\times10^{-17}$. Thus, in this simple scenario, these two experiments suggest coefficient values near $\sin^2 2\theta\simeq 0.78$ and $\Delta\mathring{c}\simeq 2.4\times10^{-17}$, in agreement with the estimates of Sec. III C.

The remaining coefficient $\delta\mathring{c}$ can then be chosen to match observed atmospheric-neutrino effects. The coefficient $\Delta\mathring{c}$ is relatively large in this region and generates rapid oscillations. Averaging over these for any value of $\delta\mathring{c}$ leaves a muon-neutrino survival probability of either $P_{\nu_\mu\to\nu_\mu}\simeq 0.54-0.27\sin^2(\delta\mathring{c}LE/2)$ or $P_{\nu_\mu\to\nu_\mu}\simeq 0.77-0.73\sin^2(\delta\mathring{c}LE/2)$, depending on the solution for θ. Note that the latter expression resembles the usual maximal-mixing solution within an overall scale factor, except for the unusual energy dependence in the oscillation length.

Interestingly, atmospheric electron-neutrino oscillations are present in this model but are largely unobserved due to a compensation mechanism. The averaged ν_e survival probability is $P_{\nu_e\to\nu_e}=61\%$, as above, and the $\nu_e\leftrightarrow\nu_\mu$ mixing probability is $P_{\nu_e\leftrightarrow\nu_\mu}=19.5\%$. The observed flux of atmospheric electron neutrinos is a combination of the survival flux and the appearance flux from mixing with muon neutrinos. Since the ratio of muon neutrinos to electron neutrinos is approximately 2, the predicted effective flux of atmospheric electron neutrinos is approximately $61\%+2(19.5\%)\simeq 100\%$ of the flux in the absence of oscillations, in agreement with indications from existing data. Essentially, this compensation mechanism works because the disappearance probability $1-P_{\nu_e\to\nu_e}$ of electron neutrinos given by Eq. (30) is a factor of two greater than the appearance probability $P_{\nu_e\leftrightarrow\nu_\mu}$ of muon neutrinos from mixing, resulting in no net suppression in the total observed electron-neutrino flux.

The compensation mechanism *per se* is independent of Lorentz violation and can be applied whenever $1-P_{\nu_e\to\nu_e}\approx 2P_{\nu_e\leftrightarrow\nu_\mu}$, including in the conventional massive case. Note, however, that Monte Carlo calculations suggest the flux ratio increases dramatically above 2 for energies over about 10 GeV [73], so the compensation mechanism is likely to fail at higher energies. Note also that, in the case of the above Lorentz-violating model, the rapid oscillations at high energies also help to mask ν_e oscillations. Although these rapid oscillations can change the overall flux, they also tend to smooth away the observable E and L dependences that form the basis for some analyses.

This simple model serves to illustrate a possible strategy that might remedy the conflict between LSND and reactor experiments, but it may well introduce other conflicts between LSND and accelerator experiments testing $\nu_e\to\nu_\tau$ and $\nu_\mu\to\nu_\tau$ [64,65] or $\nu_\mu\to\nu_e$ [66,67]. Note also that some work has been done to check for unconventional energy dependences in the atmospheric data [74], suggesting that the usual energy dependence is preferred. However, these analyses are limited to two generations and do not consider pos-

sible direction dependences or $\nu \leftrightarrow \overline{\nu}$ mixing. A complete treatment would also need to include the effects of the Earth's matter potential, which introduces additional energy dependence. The point is that $G_F n_e \sim 10^{-22}$ GeV for the Earth, and at atmospheric-neutrino energies this is comparable to the contribution from $\delta \mathring{c}$ shown in Fig. 2. In any case, interesting sensitivities to Lorentz violation could be achieved with a complete analysis of existing data.

2. Example: $(a_L)^T_{e\mu} \neq 0$, $(c_L)^{TT}_{\mu\tau} \neq 0$

We turn next to an FC model with mixed energy dependence, incorporating only two nonzero coefficients $(a_L)^T_{e\mu} \equiv \mathring{a}$ and $\frac{4}{3}(c_L)^{TT}_{\mu\tau} \equiv \mathring{c}$ and no mass terms. This case includes both Lorentz and *CPT* violation but remains rotation symmetric. The presence of both a dimensionless coefficient and a dimension-one coefficient leads to unusual energy behavior in the vacuum-mixing angles as well as the oscillation lengths. This contrasts with the previous case, in which only the oscillation lengths have unconventional energy dependence. Note that both $\mathring{a}$ and $\mathring{c}$ are arbitrary to an unobservable phase, and therefore they can be taken real and nonnegative without loss of generality.

The behavior in this model can be understood qualitatively as follows. At low energies $E \ll \mathring{a}/\mathring{c}$ relative to the critical energy $\mathring{a}/\mathring{c}$, the $\mathring{a}$ term dominates the effective Hamiltonian. As a result, ν_τ decouples from ν_e and ν_μ, so only $\nu_e \leftrightarrow \nu_\mu$ mixing occurs. In contrast, for high energies $E \gg \mathring{a}/\mathring{c}$, $\mathring{c}$ dominates and only $\nu_\mu \leftrightarrow \nu_\tau$ mixing occurs. At intermediate energies $E \sim \mathring{a}/\mathring{c}$, the two terms are comparable and produce complicated energy dependence with mixing between all three neutrinos.

This behavior is similar to the observed energy dependence in the solar-neutrino flux. In the usual analysis with massive neutrinos, the observed energy dependence is explained through matter effects. However, the same type of behavior can appear in Lorentz-violating scenarios even without matter. To demonstrate this, we need the probabilities for the current model:

$$P_{\nu_e \to \nu_e} = 1 - 4\sin^2\theta\cos^2\theta\sin^2(\pi L/L_0) - \sin^4\theta\sin^2(2\pi L/L_0), \tag{31a}$$

$$P_{\nu_\mu \to \nu_\mu} = 1 - \sin^2(2\pi L/L_0), \tag{31b}$$

$$P_{\nu_\tau \to \nu_\tau} = 1 - 4\sin^2\theta\cos^2\theta\sin^2(\pi L/L_0) - \cos^4\theta\sin^2(2\pi L/L_0), \tag{31c}$$

$$P_{\nu_e \leftrightarrow \nu_\mu} = \sin^2\theta\sin^2(2\pi L/L_0), \tag{31d}$$

$$P_{\nu_e \leftrightarrow \nu_\tau} = \sin^2\theta\cos^2\theta[4\sin^2(\pi L/L_0) - \sin^2(2\pi L/L_0)], \tag{31e}$$

$$P_{\nu_\mu \leftrightarrow \nu_\tau} = \cos^2\theta\sin^2(2\pi L/L_0), \tag{31f}$$

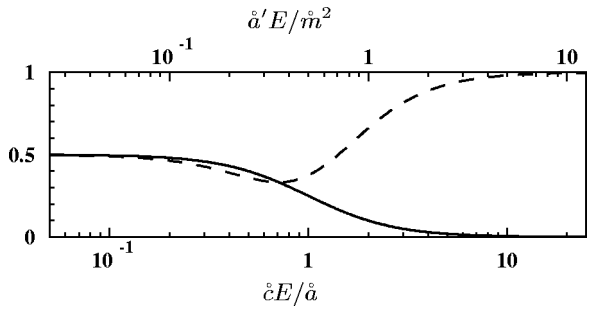

FIG. 3. Solar-neutrino survival probability assuming adiabatic propagation (solid) and average survival probability for vacuum oscillations (dashed).

where

$$\sin^2\theta = \mathring{a}^2/(\mathring{a}^2 + \mathring{c}^2E^2),$$

$$2\pi/L_0 = \sqrt{\mathring{a}^2 + \mathring{c}^2E^2}. \tag{32}$$

The antineutrino probabilities are again identical since the quantities $\sin^2\theta$ and L_0 are symmetric under $\mathring{a} \to -\mathring{a}$. We remark in passing that this model serves as an example in which *CPT* is violated but the traditional test of *CPT* discussed in Sec. II E fails as an indicator of the *CPT* violation.

The solar-neutrino vacuum-oscillation survival probability is given by Eq. (31a). As usual, depending on the size of the coefficients, matter effects can drastically alter the survival rates. Consider, for example, a simple matter-dominated case where the matter potential at the point of ν_e production dominates $h_{\rm eff}$. Assuming adiabatic propagation, neutrinos are produced in the highest-eigenvalue state of $h_{\rm eff}(R \simeq 0)$ and emerge from the Sun in the highest-eigenvalue state of $h_{\rm eff}(R = R_\odot)$. The overlap between this state and an electron-neutrino state is proportional to $\sin\theta/\sqrt{2}$. Consequently, the average survival probability for the matter-dominated case in an adiabatic approximation is

$$\langle P_{\nu_e \to \nu_e} \rangle_{\rm adiabatic} = \frac{1}{2}\sin^2\theta. \tag{33}$$

In contrast, the average for the case where matter effects can be neglected is

$$\langle P_{\nu_e \to \nu_e} \rangle_{\rm vacuum} = 1 - 2\sin^2\theta + \frac{3}{2}\sin^4\theta. \tag{34}$$

These probabilities are plotted on Fig. 3 as a function of energy in units of $\mathring{a}/\mathring{c}$.

The observed flux is consistent with the figure, since low-energy experiments suggest an approximate survival probability of 1/2 [38–40], while higher-energy experiments favor about 1/3 [37,41,42]. Note that both cases shown in Fig. 3 yield an average survival probability of 1/3 at $E = \mathring{a}/\sqrt{2}\mathring{c}$. By choosing the ratio $\mathring{a}/\mathring{c}$ to coincide with the peak of the solar ^{8}B spectrum ($E_{\rm peak} \simeq 6.4$ MeV), this simple massless Lorentz- and *CPT*-violating model can be made to

reproduce the gross features of the observed solar-neutrino flux. This corresponds to imposing $\mathring{a}/\mathring{c} \simeq 9$ MeV.

The above discussion only depends on the ratio of coefficients. To get a sense of the size of coefficients required in a realistic case, we can consider what KamLAND implies for $\mathring{a}$ and $\mathring{c}$. Taking a representative neutrino to have energy $E = 5$ MeV and baseline $L = 200$ km and assuming that it oscillates no more than once, the ratio $\mathring{a}/\mathring{c} \simeq 9$ MeV and the survival probability $P_{\bar{\nu}_e \to \bar{\nu}_e} \simeq 61\%$ can be used to extract approximate values $\mathring{a} \simeq 7 \times 10^{-22}$ GeV and $\mathring{c} \simeq 8 \times 10^{-20}$. The lines of sensitivity for these values on Fig. 1 are approximately $L \sim 10^{21}$ GeV^{-1} and $LE \sim 10^{19}$, passing just above KamLAND and intersecting in the solar-energy region, thereby producing the energy dependence seen in Fig. 3.

3. Example: $(\tilde{m}^2)_{e\mu} \neq 0$, $(a_L)^{TT}_{\mu\tau} \neq 0$

As a variation on the above model, we next consider a special FC case with nonzero mass $(\tilde{m}^2)_{e\mu} \equiv \mathring{m}^2$ and coefficient $(a_L)^{TT}_{\mu\tau} \equiv \mathring{a}'$ for Lorentz and *CPT* violation. This model has many qualitative features of the previous one. At small energies, the mass $\mathring{m}$ controls mixing between ν_e and ν_μ, while at large energies $\mathring{a}'$ dominates and produces mixing between ν_μ and ν_τ.

The probabilities for this model are given by Eqs. (31), (33), and (34), but with the definitions

$$\sin^2\theta = \mathring{m}^4/(\mathring{m}^4 + 4\mathring{a}'^2 E^2),$$

$$2\pi/L_0 = \sqrt{(\mathring{m}^2/2E)^2 + \mathring{a}'^2}. \tag{35}$$

The analysis of this model parallels the previous case. Indeed, Fig. 3 also holds for the solar-neutrino probabilities in terms of $\mathring{m}$ and $\mathring{a}'$, using the scale shown on the top axis. Applying the same arguments as before yields the ratio $\mathring{m}^2/\mathring{a}' \simeq 18$ MeV and candidate values $\mathring{m}^2 \simeq 7 \times 10^{-6}$ eV^2 and $\mathring{a}' \simeq 4 \times 10^{-22}$ GeV.

A key difference between this case and the previous $\mathring{a}$-$\mathring{c}$ model is the asymptotic behavior of the oscillation length. In the $\mathring{a}$-$\mathring{c}$ case, $L_0 \to 2\pi/(\mathring{c}E)$ at high energies. In contrast, the oscillation length in the present $\mathring{m} - \mathring{a}'$ model approaches a constant at high energies, $L_0 \to 2\pi/\mathring{a}'$. Consider the consequences for atmospheric neutrinos. Note that in the high-energy limit of both cases, $\sin^2\theta \to 0$ and so $P_{\nu_e \to \nu_e} \to 0$, in agreement with observation. However, the first model with $\mathring{c} \simeq 8 \times 10^{-20}$ gives $L_0 \simeq 2\pi/(\mathring{c}E) \simeq (15 \text{ km GeV})/E$, whereas the second model with $\mathring{a}' \simeq 4 \times 10^{-22}$ GeV yields $L_0 \simeq 3100$ km. These differ from the usual massive-neutrino explanation of the atmospheric data, which has $\Delta m^2 \simeq 3 \times 10^{-3}$ eV^2 and results in $L_0 = 4\pi E/\Delta m^2 \simeq 800E$ km/GeV.

We emphasize that both this special model and the previous one involve only two degrees of freedom, whereas the usual massive-neutrino solution requires two mass-squared differences and at least two mixing angles. Including additional coefficients for Lorentz violation can only add flexibility to the analysis. For example, one might consider a combination of the two examples above, which would have four degrees of freedom. With additional freedom, it seems likely that an appropriate simple Lorentz-violating scenario could be constructed that would reproduce most oscillation data. This also suggests that existing data analyses appear insufficient to exclude many forms of Lorentz and *CPT* violation, or even to distinguish between oscillations due to mass and those due to Lorentz violation.

B. Direction-dependent and $\nu \leftrightarrow \bar{\nu}$ mixing models

Lorentz violation naturally allows directional dependence in oscillation parameters through the violation of rotation invariance. An interesting subset of direction-dependent models are those involving $\nu \leftrightarrow \bar{\nu}$ mixing via nonzero $g^{\mu\nu\sigma}$ and $H^{\mu\nu}$ coefficients in the theory (14). In the general case, nonzero $\nu \leftrightarrow \bar{\nu}$ mixing represents one way to generate as many as five distinct oscillation lengths without incorporating sterile neutrinos. However, we limit attention in this subsection to a simple model that reveals some key features of $\nu \leftrightarrow \bar{\nu}$ mixing. For illustrative purposes, it suffices to consider mixing in only one neutrino species, say $\nu_e \leftrightarrow \bar{\nu}_e$. This case may nonetheless have physical relevance, since it implies significant effects on reactor experiments and solar neutrinos and might possibly also shed light on the LSND anomaly.

1. General one-species model

The restriction to the two-dimensional ν_e-$\bar{\nu}_e$ subspace radically simplifies the form of the effective Hamiltonian (14). Since the coefficients $(\tilde{m}^2)_{ee}$ and $(c_L)_{ee}$ are real, they lead to terms proportional to the identity that have no effect on oscillatory behavior and can therefore be ignored. Moreover, Eq. (4) implies that $(H^{\mu\nu}\mathcal{C})_{ab}$ is antisymmetric in generation space, so $(H^{\mu\nu}\mathcal{C})_{ee} = H^{\mu\nu}_{ee^C} = 0$. Therefore, the most general single-flavor theory without mass differences is given by a 2×2 effective Hamiltonian containing only the coefficients $(a_L)^\mu_{ee}$ and $(g^{\mu\nu\sigma}\mathcal{C})_{ee} = g^{\mu\nu\sigma}_{ee^C}$ for Lorentz violation. Note that both these terms are *CPT* odd.

For this general single-flavor model, the probabilities are identical in form to those of the usual two-generation mixing case

$$P_{\nu_e \leftrightarrow \bar{\nu}_e} = 1 - P_{\nu_e \to \nu_e} = 1 - P_{\bar{\nu}_e \to \bar{\nu}_e}$$
$$= \sin^2 2\theta \sin^2 2\pi L/L_0. \tag{36}$$

However, the mixing angle and oscillation length can have nontrivial four-momentum dependence. They are given by the expressions

$$\left(\frac{2\pi}{L_0}\right)^2 = \frac{|(a_L)^\mu_{ee} p_\mu|^2}{|\vec{p}|^2} + |\sqrt{2}(\epsilon_+)_\nu p_\sigma \tilde{g}^{\nu\sigma}_{ee^C}|^2,$$

$$\sin^2 2\theta = \left(1 + \frac{|(a_L)^\mu_{ee} p_\mu|^2}{|\vec{p}|^2 |\sqrt{2}(\epsilon_+)_\nu p_\sigma \tilde{g}^{\nu\sigma}_{ee^C}|^2}\right)^{-1}. \tag{37}$$

Note that these can also be written directly in terms of the neutrino-propagation angles Θ and Φ defined in Eq. (25).

2. Example: $\tilde{g}^{ZT}_{ee^C} \neq 0$

As an explicit example, we consider a maximal-mixing special case of the general single-flavor model for which the only nonzero coefficient is $\tilde{g}^{ZT}_{ee^C} \equiv \check{g}$. In terms of the propagation angles Θ and Φ, the oscillation length is found to be

$$2\pi/L_0 = |E \sin\Theta \check{g}|, \tag{38}$$

and the mixing angle is $\sin^2 2\theta = 1$. As in the previous examples, this case has unconventional energy dependence, but unlike previous examples it includes neutrino-antineutrino mixing and also dependence on the direction of propagation through the propagation angle Θ.

To illustrate the effects of the direction dependence, consider atmospheric neutrinos detected in the SK detector. Neutrinos that enter the detector from the celestial north or south have $\sin\Theta = 0$ and therefore do not oscillate. In contrast, neutrinos propagating in the plane parallel to the Earth's equatorial plane have $\sin\Theta = 1$ and experience maximal mixing [75]. Analyses of SK data often neglect the difference between ν_e and $\bar{\nu}_e$, so they may be insensitive to this effect because the total flux of electron neutrinos and antineutrinos is unchanged. However, the same type of directional dependence can arise in more complicated scenarios with $\nu_e \leftrightarrow \nu_\mu \leftrightarrow \nu_\tau$ mixing, and this could drastically affect the up-down asymmetry measurements of SK.

As another example consider KamLAND, which detects neutrinos from several reactors at different locations. The total flux $\phi_{\text{total}}(E)$ of $\bar{\nu}_e$ can be written

$$\phi_{\text{total}}(E) = \sum_j \phi_j(E) P_{\bar{\nu}_e \to \bar{\nu}_e}(E, L_j, \Theta_j), \tag{39}$$

where the $\phi_j(E)$ are the fluxes from the individual reactors in the absence of oscillations, and Θ_j are appropriate propagation angles determined by the relative positions of the reactors and the KamLAND detector. We can approximate the positions of the reactors as being located in the plane tangent to the surface of the Earth at the location of the detector. It follows that neutrinos from reactors positioned directly north and south of the detector have $\Theta_j \simeq 180° - \chi$ and $\Theta_j \simeq \chi$, where $\chi \simeq 36°$ is the latitude of the detector. In contrast, neutrinos arriving from the east or west have $\Theta_j \simeq 90°$. This results in an approximate allowed range for the Θ_j given by $\sin^2\Theta_j \gtrsim \sin^2\chi$, implying that the $\bar{\nu}_e$ from every reactor experience some degree of oscillation on their way to the KamLAND detector. However, the net result differs from the flux in a comparable rotation-symmetric model with a dimensionless coefficient.

For solar neutrinos, the allowed range for Θ is given by $\sin^2\Theta \gtrsim \cos^2\eta \simeq 0.85$ because the Earth's orbital and equatorial planes differ by approximately $\eta = 23°$. The true value of $\sin^2\Theta$ oscillates between $\sin^2\Theta = 1$ in the spring or fall and $\sin^2\Theta \simeq 0.85$ in the summer or winter. This simple model therefore predicts a semiannual variation in the solar-neutrino data.

As suggested in Sec. III C, oscillations of ν_e into $\bar{\nu}_e$ may provide an alternative approach to resolving the LSND anomaly. If the LSND result is reinterpreted as an oscillation of ν_e into $\bar{\nu}_e$, then the transition probability is likely to be comparable to the reported value of about 0.26% because roughly equal numbers of ν_e and $\bar{\nu}_\mu$ are produced. Since mixing in this model is caused by the dimensionless coefficient $\check{g}$, a reasonable strategy here is similar to that adopted for the $\delta\mathring{c} - \Delta\mathring{c}$ model in Sec. IV A 1, where a dimensionless coefficient is chosen to have its line of sensitivity just above CHOOZ and LSND in Fig. 1. This causes a small oscillation in LSND but avoids the null constraints from reactor experiments. Taking the energy of a typical ν_e to be about $E = 35$ MeV and the distance to be $L = 30$ m in LSND, and assuming that the small transition probability is due to a small L/L_0, we can write $P_{\nu_e \to \bar{\nu}_e} = \sin^2 2\theta \sin^2 2\pi L/L_0 \simeq (\sin\Theta \check{g} L E)^2 \simeq 0.26\%$. For LSND, the detector is situated approximately to the east of the source. This implies that the angle between celestial north and the direction of propagation of the neutrinos is near 90°, which results in the estimate $|\check{g}| \simeq 10^{-17}$.

In contrast, the KARMEN detector is located roughly to the south of the neutrino source, at latitude $\chi \simeq 51°$. We can therefore approximate $\Theta \simeq 180° - \chi \simeq 129°$. Taking $E = 35$ MeV and $L = 18$ m for KARMEN yields a transition probability $P_{\nu_e \to \bar{\nu}_e} = \sin^2 2\theta \sin^2 2\pi L/L_0 \simeq (\sin\Theta \check{g} L E)^2 \simeq 0.06\%$. This is more than four times smaller than the LSND probability as a consequence of the different propagation direction and the smaller distance, confirming that direction dependence could help reconcile the apparent conflict between KARMEN and LSND.

In the above model, the directional dependence is rather limited because the coefficient $\check{g}$ introduces only Θ dependence. This causes minimal variation for any experiments with both neutrino source and detector fixed on the Earth's surface, since the angle Θ is fixed as the Earth rotates and is therefore a constant experiment-dependent quantity. However, other coefficients can produce a strong dependence on Φ as well. For instance, suppose we choose $\tilde{g}^{ZX}_{ee^C}$ instead of $\tilde{g}^{ZT}_{ee^C}$. The result is an oscillation length given by $2\pi/L_0 = |E \sin^2\Theta \cos\Phi \tilde{g}^{ZX}_{ee^C}|$. The dependence on Φ can substantially change the nature of an experiment. For purely terrestrial experiments, where the source and detector are fixed to the surface of the Earth, it follows that $\Phi = \omega_\oplus (T - T_0)$, where $\omega_\oplus \simeq 2\pi/(23\text{ h }56\text{ min})$ is the Earth's sidereal frequency and T_0 is an appropriately chosen experiment-dependent offset. For solar neutrinos, Φ varies as the Earth orbits the Sun, $\Phi \approx \Omega_\oplus (T - T_0)$, where $\Omega_\oplus = 2\pi/(1\text{ year})$.

C. Lorentz-violating seesaw models

The above models demonstrate some of the striking behavior at different energy scales that can arise from Lorentz and *CPT* violation. Mixed energy dependence among the co-

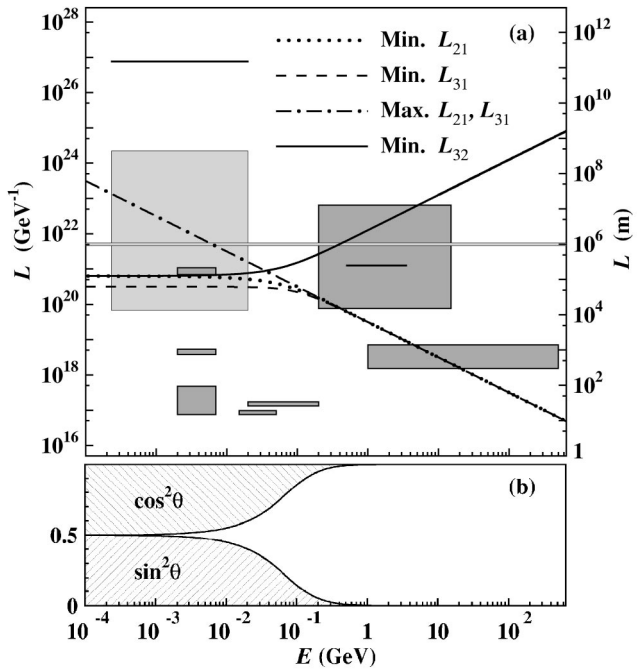

FIG. 4. Range of oscillation parameters versus energy in the bicycle model with $\mathring{c}=10^{-19}$ and $\breve{a}=10^{-20}$ GeV. (a) Minimum ($\cos^2\Theta=1$) and maximum ($\cos^2\Theta=0$) of the various oscillation lengths $L_{ab}\equiv 2\pi/\Delta_{ab}$. Note that L_{32} is unbounded. (b) The allowed range of $\sin^2\theta$ and $\cos^2\theta$ over all possible directions, $0\leqslant\cos^2\Theta\leqslant 1$, as a function of energy.

efficients for Lorentz violation in $h_{\rm eff}$ can also lead to a Lorentz-violating seesaw mechanism that occurs without mass and only in particular energy regimes. This can lead to counterintuitive phenomena, such as the appearance of a pseudomass in the bicycle model of Ref. [29]. In this model, an oscillation length emerges at high energies that behaves similar to a mass-squared difference, even though no mass-squared differences exist in the theory.

The bicycle model has nonzero coefficients $\frac{4}{3}(c_L)^{TT}_{ee}=\frac{4}{3}(c_L)^{JJ}_{ee}\equiv 2\mathring{c}$ and $(a_L)^Z_{e\mu}=(a_L)^Z_{e\tau}\equiv\breve{a}/\sqrt{2}$. The basic behavior of the oscillation lengths $L_{ab}\equiv 2\pi/\Delta_{ab}$ and the energy-dependent mixing angle θ are illustrated in Fig. 4. A key feature is that at high energies the line associated with the oscillation length L_{32} resembles that from a nonzero mass-squared difference. It turns out that the resulting high-energy dynamics reduces to two-generation maximal mixing, $P_{\nu_\mu\leftrightarrow\nu_\tau}\simeq\sin^2(\Delta m^2_\Theta L/4E)$, with a Lorentz- and CPT-violating pseudomass $\Delta m^2_\Theta=\breve{a}^2\cos^2\Theta/\mathring{c}$.

Unexpected effects of this type can be expected whenever the low- or high-energy limit of $h_{\rm eff}$ contains degeneracies. Consider, for example, a 3×3 Hamiltonian $h_{\rm eff}$ for which there exists a basis, not necessarily the flavor basis, in which we can write

$$h_{\rm eff}=\begin{pmatrix} 2h_1 & h_2 & h_3 \\ h_2^* & 0 & 0 \\ h_3^* & 0 & 0 \end{pmatrix}, \tag{40}$$

where irrelevant diagonal terms are neglected. The interesting eigenvalue difference for this case is $\Delta=\sqrt{(h_1)^2+|h_2|^2+|h_3|^2}-h_1$. Suppose that the mixed energy dependence introduced by combinations of masses, dimension-one coefficients, and dimensionless coefficients enforces $h_1\gg\sqrt{|h_2|^2+|h_3|^2}$ at some energy scale. Expanding the eigenvalue difference then yields [76] $\Delta\approx\frac{1}{2}(|h_2|^2+|h_3|^2)/h_1+\cdots$.

In the bicycle model, h_2 and h_3 arise from a dimension-one coefficient and are therefore constant with energy, but h_1 arises from a dimensionless coefficient and therefore grows linearly with energy. As a result, at high energies the eigenvalue difference is proportional to E^{-1}, which resembles the usual mass case. Using different combinations of masses and coefficients for Lorentz violation, it is straightforward to construct similar models that produce E^{-1}, E^{-2}, or E^{-3} dependence at high energies, or E^1, E^2, or E^3 dependence at low energies. More complicated E^n dependences are possible when the full 6×6 effective Hamiltonian (14) with $\nu\leftrightarrow\overline{\nu}$ mixing is considered.

V. DISCUSSION

In this paper, we have presented a general framework for the study of Lorentz violation in the neutrino sector. The key result is Eq. (14), which represents the general effective Hamiltonian $h_{\rm eff}$ for neutrino propagation in the presence of Lorentz and *CPT* violation. We have extracted theoretical implications of this Hamiltonian and have initiated a study of experimental sensitivities to the predicted effects. The various simple models of Sec. IV illustrate some of the key physical features and offer numerous options for future exploration.

Our analysis shows that the data from existing and near-future neutrino experiments could be used to attain interesting sensitivities to possible Lorentz-violating effects. Moreover, the existing analyses appear insufficient to exclude the possibility that some or perhaps even all the established neutrino-oscillation signals are due to Lorentz violation.

An interesting open theoretical challenge is to identify from the plethora of available choices one or more elegant models with features compatible with observed data, preferably involving only a small number of degrees of freedom. One simple candidate is the bicycle model [29], which has no mass-squared differences and only two degrees of freedom rather than the four used in the conventional massive-neutrino analysis, but which nonetheless reproduces the major observed features of neutrino behavior. This and similar models offer one possible path to explore, but it is likely that many other qualitatively different and interesting cases exist.

On the experimental front, confirming or disproving these ideas would involve analysis of existing and future data to seek a ''smoking-gun'' signal for Lorentz violation. In the remainder of this section, we summarize some possible smoking-gun signals and then offer some remarks about experimental prospects for detection of Lorentz and *CPT* violation.

A. Generic predictions

The numerous options for coefficients for Lorentz and *CPT* violation and the size of unexplored L versus E space are impediments to a completely general analysis. An alternative strategy to uncover evidence of Lorentz violation is to seek model-independent features that represent characteristic signals. We list here six classes of signal. Confirmed observation of any of them would be evidence supporting the existence of Lorentz violation.

Class I: Spectral anomalies. Each coefficient for Lorentz violation introduces energy dependence differing from the usual case. Detection of a vacuum oscillation length that is constant in E or inversely proportional to E to some power would constitute a clear signal of Lorentz violation. Note that combinations of masses, dimension-one coefficients, dimensionless coefficients, and matter potentials can produce more complicated energy dependences in both oscillation lengths and mixing angles. In general, a mixing angle is constant in energy only if all relevant coefficients for Lorentz violation, masses, and matter effects have the same dimension, which requires no more than one of these to be present.

Class II: L-E conflicts. This class of signal refers to any null or positive measurement in a region of L-E space that conflicts with all scenarios based on mass-squared differences. For example, consider a solid line in Fig. 1 passing through CHOOZ. A measurement of substantial oscillation in the $\overline{\nu}_e$ sector in any experiment below this line would be in direct conflict with a mass-based interpretation of the CHOOZ results. Signals in this class might best be sought by searching for oscillation effects in each species of neutrino and antineutrino for regions of L-E space in which conventional oscillations are excluded. Of the six classes of signal discussed in this section, this is the only one for which there is presently some positive evidence, the LSND anomaly.

Class III: Periodic variations. This class involves signals for rotation-invariance violations and contains two subclasses: sidereal variations and annual variations. Consider first sidereal variations, which have been widely adopted as the basis for Lorentz-violation searches in other sectors of the SME. In terrestrial experiments with both the detector and the source fixed on the Earth, the direction of neutrino propagation relative to the Sun-centered frame changes during the sidereal day due to the rotation of the Earth. The induced periodic variation of observables with time represents a signature of Lorentz violation. In the Sun-centered frame, the neutrino-propagation angle Θ is constant for a fixed source, but the angle Φ varies periodically according to $\Phi=\omega_\oplus(T-T_0)$, where T_0 is an experiment-dependent time at which the detector and source both lie in a plane parallel to the XZ plane with the detector at larger values of X. The resulting neutrino-oscillation probabilities exhibit periodic variations at multiples of the sidereal frequency $\omega_\oplus$. The second class of periodic signals, annual variations, can also arise directly from rotation-invariance violation. For solar-neutrino experiments, the source is the Sun and the detector changes location with time as a consequence of the orbital motion of the Earth about the Sun. One can therefore expect variations at the Earth orbital frequency $\Omega_\oplus$ and its harmonics. In this context, note that the direction $\hat{p}$ of solar neutrino propagation in the Sun-centered frame is uniquely given by $\hat{p}=(-\cos\Omega_\oplus T,-\cos\eta\sin\Omega_\oplus T,-\sin\eta\sin\Omega_\oplus T)$, where $\eta\simeq 23.4°$ is the angle between the Earth's equatorial and orbital planes. We remark in passing that suppressed annual variations can also arise indirectly as boost-violating effects [15,16,21,22] in experiments with terrestrial and possibly atmospheric neutrino sources, as a result of the noninertial nature of the Earth's motion around the Sun.

Class IV: Compass asymmetries. This class also results from rotation-invariance violations, but the signals are independent of time. They can be characterized as the observation of unexplained directional asymmetries at the location of the detector. For terrestrial and atmospheric experiments, averaging over time eliminates the dependence on the neutrino-propagation angle Φ, so the result depends only on energy and the angle Θ. Rotation-symmetry violations can therefore cause a difference in observed properties of neutrinos originating from different directions. Note that the east and west directions are equivalent under the averaging process, since the Φ dependence is eliminated, but direct comparison of the north, south, and east directions would be of interest for these signals. Note also that the Θ dependence typically introduces vertical up-down effects and could include, for example, modifications in the up-down asymmetry of atmospheric neutrinos. We remark also that compass asymmetries can carry information completely independent of the information in periodic variations. This is seen in the example in Sec. IV B 2, which has Θ dependence but no Φ dependence and consequently predicts compass asymmetries without sidereal variations.

Class V: Neutrino-antineutrino mixing. This class of signal includes any appearance measurement that can be traced to $\nu\leftrightarrow\overline{\nu}$ oscillation. Any model with nonzero coefficients of type g or H exhibits this behavior, including the class of simple one-species models discussed in Sec. IV B 1. Note that this class of signal involves lepton-number violation.

Class VI: Classic CPT test: $P_{\nu_b\to\nu_a}\neq P_{\overline{\nu}_a\to\overline{\nu}_b}$. This is the traditional test of *CPT* discussed in Sec. II E, involving violation of the result (24a). A related signal would be violation of the second result, Eq. (24b), which also involves $\nu\leftrightarrow\overline{\nu}$ mixing.

B. Experimental prospects

We conclude with some comments about prospects for Lorentz- and *CPT*-violation searches in the major types of experiments. Table I provides a summary of the present situation. The left-hand part of the table contains three columns with information about coefficients for Lorentz violation. The first column lists combinations of coefficient matrices relevant to neutrino propagation, extracted from the general Hamiltonian (14) and separated according to rotation properties into timelike (T) and spacelike (J) components in the Sun-centered frame. The second column lists the maximum number of independent degrees of freedom (DOF) associated with each combination of coefficient matrices. These numbers can be obtained by examining the form of Eq. (14) and using the symmetry properties in generation space listed in

TABLE I. Experimental prospects.

Coefficients			Estimated sensitivities from Fig. (1)				
Matrix	DOF	Signal classes	Solar	Atmospheric	Reactor	Short base.	Long base.
$(a_L)^T$	8	I,II,VI	-27	-23	-21	-19	-21
$(a_L)^J$	24	I,II,III,IV,VI	-27	-23	-21	-19	-21
$(c_L)^{TT}=(c_L)^{JJ}$	8	I,II	-25	-24	-19	-21	-22
$\frac{1}{2}(c_L)^{(TJ)}$	24	I,II,III,IV	-25	-24	-19	-21	-22
$\frac{1}{2}(c_L)^{(JK)}-\frac{1}{3}\delta^{JK}(c_L)^{TT}$	40	I,II,III,IV	-25	-24	-19	-21	-22
$\tilde{g}^{JT}-\frac{i}{2}\epsilon^{JKL}\tilde{g}^{KL}$	36	I,II,III,IV,V,VI	-25	-24	-19	-21	-22
$\frac{1}{2}\tilde{g}^{(JK)}-\frac{1}{3}\delta^{JK}\tilde{g}^{LL}$	60	I,II,III,IV,V,VI	-25	-24	-19	-21	-22
$\tilde{H}^J$	18	I,II,III,IV,V	-27	-23	-21	-19	-21
$(k_d)^{\lambda\cdots}$	var.	I,II,III,IV,V,VI	$-27+2d$	$-23-d$	$-21+2d$	$-19-2d$	$-21-d$

Eq. (4). In certain specific models, some of these degrees of freedom may be unobservable. The third column displays the classes of signal that are relevant for each coefficient matrix, using the nomenclature of the previous subsection. The right-hand part of the table contains estimated attainable sensitivities, classified according to each of five types of oscillation experiments. Each entry in the table represents the base-10 logarithm of the expected sensitivity to the corresponding coefficient for Lorentz violation. The sensitivities shown in the table can be obtained by examination of Fig. 1. Given an experiment with maximum L coverage of $L_{\max}$ and maximum E coverage of $E_{\max}$, the crude sensitivity σ to a coefficient for Lorentz violation of dimension $1-d$ is taken to be $\sigma \approx -\log L_{\max} - d\log E_{\max}$. For simplicity in the presentation, it is understood that the sensitivities listed for the dimension-one coefficients a_L, H are measured in GeV. The final row of the table contains a rough estimate of sensitivities measured in $\mathrm{GeV}^{(1-d)}$ to a generic coefficient $(k_d)_{\lambda\cdots}$ for a Lorentz-violating operator of nonrenormalizable dimension $n=d+3$. Some caution is required in interpreting the latter numerical estimates because the coefficients $(k_d)_{\lambda\cdots}$ are expected typically to be suppressed by d-dependent powers of the Planck scale.

The table confirms that Planck-scale sensitivities to Lorentz and *CPT* violation are attainable in all classes of experiment, with the most sensitive cases potentially rivaling the best tests in other sectors of the SME. Note that the estimated sensitivities assume order-one measurements and therefore may underestimate the true attainable sensitivity in any specific experiment. Note also that a variety of experimental analyses are needed to extract complete information on Lorentz and *CPT* violation, with no single class of experiment presently in a position to provide measurements of a complete set of coefficients. In the remainder of this subsection, we offer a few more specific remarks about each type of experiment.

Solar-neutrino experiments. The abundance and quality of the current solar-neutrino data make these experiments a promising avenue for Lorentz-violation searches. The relatively large range of solar-neutrino energies suggests interesting information about spectral anomalies might be obtained, but complications introduced by matter effects are likely to make this practical only in relatively simple cases such as the FC model (28). Of the other classes of signals, periodic variations and neutrino-antineutrino mixing may be the most relevant to solar neutrinos. The periodic variations in observables would occur at multiples of $\Omega_\oplus$, appearing despite compensation for the flux variation due to the eccentricity of the Earth's orbit. Direct detection of any antineutrinos originating from the Sun would be evidence of $\nu \leftrightarrow \overline{\nu}$ mixing and hence of possible Lorentz violation.

Atmospheric-neutrino experiments. Similar to solar neutrinos, atmospheric neutrinos cover a relatively large region of L-E space, but complications from matter effects hinder a general spectral-anomaly search. However, Fig. 2 shows that searches for atmospheric oscillations at the highest energies and largest distances could reveal oscillations absent in the usual solution, thereby providing evidence for L-E conflicts. Atmospheric neutrinos originate from all directions, so they are an ideal system for directional-dependence searches. Not only are they sensitive to sidereal variations, but also the directional capabilities of detectors such as SK make atmospheric neutrinos perhaps the most promising place to search for compass asymmetries. Moreover, since atmospheric data involve both neutrinos and antineutrinos of two species in comparable numbers, it may be possible to address both $\nu \leftrightarrow \overline{\nu}$ mixing and the classic *CPT* tests (24a) and (24b).

Reactor experiments. Nuclear reactors are good sources of $\overline{\nu}_e$, and they are therefore well suited to searches for $\nu \leftrightarrow \overline{\nu}$ mixing. Since both the sources and the detectors in all these cases are fixed, the experiments are also sensitive to sidereal variations, and some may have additional sensitivity to compass asymmetries. For example, the reactor experiment KamLAND detected neutrinos from multiple reactors and different locations. Experiments with multiple sources such to this can analyze their data for compass asymmetries that depend on the direction to the various neutrino sources.

Short-baseline accelerator experiments. LSND already seems to suggest a positive L-E conflict, which will be tested by the forthcoming results of the MiniBooNE experiment. Many of these short-baseline accelerator experiments are especially interesting for signals based on L-E conflicts because they operate in a region of L-E space where the con-

ventional mass scenario predicts no oscillations. Sidereal variations can readily be sought by experiments such as CHORUS, KARMEN, MiniBooNE, NOMAD, and NuTeV, since each has a fixed source and detector. Note that the existing data from these experiments could in principle contain a positive signal for sidereal variations because the published null results are based on an average over time. The well-defined flavor content of the sources for these experiments may also offer sensitivity to $\nu \leftrightarrow \overline{\nu}$ signals and to the classic *CPT* test. Some of these experiments, such as MiniBooNE and NuTeV, may be particularly sensitive to Lorentz violation because they can switch from a predominately ν_μ source to a predominately $\overline{\nu}_\mu$ source.

Long-baseline accelerator experiments. Several future long-baseline accelerator-based experiments, such as ICARUS, MINOS, and OPERA, are planned to probe the GeV region of L-E space at distances of hundreds of kilometers, and some results in this regime have already been reported by K2K. These experiments can search for oscillations in ν_μ obtained from meson decays, and they are designed to test the atmospheric-oscillation hypothesis. Nonetheless, L-E conflicts are still possible: a measurement of $\nu_\mu \to \nu_e$, for example, would represent an $L-E$ conflict because this oscillation is absent at these energies and distances in the conventional scenario with masses. The data obtained can be also analyzed for sidereal variations, since in each case the source and detector are fixed. Moreover, except for OPERA and ICARUS, which are both part of the CERN Neutrinos to Gran Sasso (CNGS) project, the beamline for each experiment points in a different direction. This means each is expected to respond differently to rotation-invariance violations. These experiments may also be able to address $\nu \leftrightarrow \overline{\nu}$ mixing and the classic *CPT* signal, since the flavor content of the beams is well known.

Other experiments. Experiments designed to search for neutrino properties other than oscillations can also address Lorentz violation. To some extent, most experiments are sensitive to sidereal variations and compass asymmetries. The other signals discussed in Sec. V A are more unique to neutrino oscillations, but analogous signatures are likely to arise in most cases.

One possible test of Lorentz invariance involves a direct comparison of velocities of supernova neutrinos and photons, such as those from SN1987A [34,77], which could be performed either by some of the experiments listed above or by neutrino telescopes. A similar method has been applied in the photon sector, where the velocities of different polarizations are compared [22]. Another method that could be adapted to the neutrino case is a simple pulse-dispersion analysis. The energy dependence and the independent propagation of each $h_{\rm eff}$ eigenstate imply that different components of the neutrino pulse propagate at different velocities, causing the pulse to spread. For SN1987A, all the observed neutrinos arrived in a time interval of about $\delta T \simeq 10$ s and had energies $E \simeq 10-20$ MeV. Since these neutrinos took roughly $T_0 \simeq 5\times 10^{12}$ s to reach the Earth, we can crudely estimate that the maximum difference in velocity across the $\Delta E \simeq 10$ MeV energy spread of the $h_{\rm eff}$ eigenstates is $\delta v/c \simeq \delta T/T_0 \simeq 2\times 10^{-12}$. We can then make a simple dimensional estimate of the sensitivity of this method to various terms in $h_{\rm eff}$. This suggests a sensitivity of about $\sqrt{200}$ eV to mass terms, 2×10^{-14} GeV to dimension-one coefficients, and 2×10^{-12} to dimensionless coefficients. The mass estimate agrees with the result of a detailed analysis along these lines [78].

Lorentz violation may also be relevant to direct mass searches such as the proposed KATRIN experiment [32], designed to measure directly the ν_e mass to better than 1 eV. Within the currently accepted solution to the oscillation data, a mass matrix with eV-scale masses but mass-squared differences of 10^{-3} eV^2 and 10^{-5} eV^2 would be nearly degenerate. This seems unlikely in light of the charged-lepton mass hierarchies. However, suppose that the mass matrix is nearly diagonal and that neutrino oscillations are primarily or entirely due to Lorentz violation instead. Then, individual masses of eV order or greater may be present with little or no effect on the existing neutrino-oscillation data, but they would produce a signal in the KATRIN experiment.

Another area of widespread interest is the search for neutrinoless double-beta decay [33]. This decay mode is an indicator of lepton-number violation, which can result from Majorana-type couplings introduced by Majorana masses or by gauge-violating coefficients for Lorentz violation. Many of the null results of searches for neutrinoless double-beta decay could therefore be reanalyzed to yield constraints on certain types of Lorentz violation.

ACKNOWLEDGMENTS

This work was supported in part by the United States Department of Energy under Grant No. DE-FG02-91ER40661 and by the National Aeronautics and Space Administration under Grant No. NAG8-1770.

APPENDIX A: EFFECTIVE HAMILTONIAN

This appendix presents some details for the derivation of the effective Hamiltonian (14). We first perform a spinor decomposition of the Hamiltonian in the mass-diagonal Majorana basis. The result is then block diagonalized in the light-neutrino sector and transformed into the original weak-interaction basis. We remind the reader that generation indices in the mass-diagonal basis are $A' = 1, \ldots, 6$ for $N = 3$ neutrino species, while the restriction to light neutrinos in this basis is represented by indices $a' = 1,2,3$. Also, in the flavor basis, upper-case indices take the values $A = e, \mu, \tau, e^C, \mu^C, \tau^C$, while lower-case ones span $a = e, \mu, \tau$.

1. Spinor decomposition

In this section, we project the Hamiltonian onto the massless spinor basis used in Eq. (10). This corresponds to choosing a convenient $\vec{p}$-dependent γ-matrix basis that allows us to write the equations of motion in terms of the b and d amplitudes.

Working in the mass-diagonal basis, the Hamiltonian is given by

$$\mathcal{H}_{A'B'}(\vec{p}) = \mathcal{H}_{0A'B'}(\vec{p}) + \delta\mathcal{H}_{A'B'}(\vec{p}),$$

$$\mathcal{H}_{0A'B'}(\vec{p}) = \gamma^0(\vec{\gamma}\cdot\vec{p} + m_{(A')})\,\delta_{A'B'},$$

$$\delta\mathcal{H}_{A'B'}(\vec{p}) = -\frac{1}{2}[\gamma^0\delta\Gamma^0\mathcal{H}_0(\vec{p}) + \mathcal{H}_0(\vec{p})\gamma^0\delta\Gamma^0]_{A'B'} + \gamma^0(\delta\vec{\Gamma}\cdot\vec{p} + \delta M)_{A'B'}. \tag{A1}$$

It turns out to be useful to decompose $\Gamma^{\mu}_{A'B'}$ and $M_{A'B'}$ in terms of γ matrices, as in Eq. (2). Therefore, we write

$$\begin{aligned}\Gamma^{\nu}_{A'B'} &= \gamma^0 U_{A'A}\gamma^0\Gamma^{\nu}_{AB}(U_{B'B})^{\dagger}\\ &= \gamma^{\nu}\delta_{A'B'} + c^{\mu\nu}_{A'B'}\gamma_{\mu} + d^{\mu\nu}_{A'B'}\gamma_5\gamma_{\mu} + e^{\nu}_{A'B'}\\ &\quad + if^{\nu}_{A'B'}\gamma_5 + \frac{1}{2}g^{\lambda\mu\nu}_{A'B'}\sigma_{\lambda\mu},\\ M_{A'B'} &= \gamma^0 U_{A'A}\gamma^0 M_{AB}(U_{B'B})^{\dagger}\\ &= m_{A'B'} + im_{5A'B'}\gamma_5 + a^{\mu}_{A'B'}\gamma_{\mu} + b^{\mu}_{A'B'}\gamma_5\gamma_{\mu}\\ &\quad + \frac{1}{2}H^{\mu\nu}_{A'B'}\sigma_{\mu\nu}.\end{aligned} \tag{A2}$$

We begin the spinor decomposition of the Hamiltonian (A1) by considering the Lorentz-covariant terms. The properties of the massless spinor basis imply that the only nonzero projections of the kinetic term are

$$\begin{aligned}u^{\dagger}_{L,R}(\vec{p})(\gamma^0\vec{\gamma}\cdot\vec{p}\quad\delta_{A'B'})u_{L,R}(\vec{p})\\ = -v^{\dagger}_{R,L}(-\vec{p})(\gamma^0\vec{\gamma}\cdot\vec{p}\quad\delta_{A'B'})v_{R,L}(-\vec{p})\\ = |\vec{p}|\,\delta_{A'B'},\end{aligned} \tag{A3}$$

while the surviving projections of the mass term are

$$\begin{aligned}u^{\dagger}_{L,R}(\vec{p})(\gamma^0 m_{(A')}\delta_{A'B'})v_{R,L}(-\vec{p})\\ = \overline{u}_{L,R}(\vec{p})v_{R,L}(-\vec{p})m_{(A')}\delta_{A'B'}\end{aligned} \tag{A4}$$

and conjugates. The quantities $\overline{u}_{L,R}(\vec{p})v_{R,L}(-\vec{p})$ are phases that can be chosen arbitrarily by changing the relative phase between $u_{L,R}(\vec{p})$ and $v_{R,L}(-\vec{p}) = C\overline{u}^{T}_{L,R}(-\vec{p})$.

For the spinor decomposition of the Lorentz-violating terms in the Hamiltonian (A1), we define the 2×2 matrices

$$\Lambda_{A'B'}(\vec{p}) = \Lambda^{\dagger}_{B'A'}(\vec{p}) = \begin{pmatrix} u^{\dagger}_L(\vec{p}) \\ u^{\dagger}_R(\vec{p})\end{pmatrix}\delta\mathcal{H}_{A'B'}(\vec{p})[u_L(\vec{p}), u_R(\vec{p})], \tag{A5}$$

$$\begin{aligned}\tilde{\Lambda}_{A'B'}(\vec{p}) = -\tilde{\Lambda}^{T}_{B'A'}(-\vec{p}) = \begin{pmatrix} u^{\dagger}_L(\vec{p}) \\ u^{\dagger}_R(\vec{p})\end{pmatrix}\delta\mathcal{H}_{A'B'}(\vec{p})\\ \times[v_R(-\vec{p}), v_L(-\vec{p})].\end{aligned} \tag{A6}$$

It can be shown that the mass-basis analogs of the relations (3) are $\Gamma^{\nu}_{A'B'} = -C(\Gamma^{\nu}_{B'A'})^{T}C^{-1}$ and $M_{A'B'} = C(M_{B'A'})^{T}C^{-1}$. Note that this corresponds to $\mathcal{C}\to I$, which reflects the Majorana nature of neutrinos in this basis. These identities may then be used to show that $C^{\dagger}\gamma^0\mathcal{H}_{A'B'}(\vec{p})\gamma^0 C = -[\mathcal{H}_{A'B'}(-\vec{p})]^{*}$. Finally, with the aid of the relation $v_{R,L}(\vec{p}) = C\overline{u}^{T}_{L,R}(\vec{p})$, it follows that the remaining terms in the spinor decomposition are given in terms of Λ and $\tilde{\Lambda}$ by

$$-\tilde{\Lambda}^{*}_{A'B'}(-\vec{p}) = \begin{pmatrix} v^{\dagger}_R(-\vec{p}) \\ v^{\dagger}_L(-\vec{p})\end{pmatrix}\delta\mathcal{H}_{A'B'}(\vec{p})[u_L(\vec{p}), u_R(\vec{p})], \tag{A7}$$

$$\begin{aligned}-\Lambda^{*}_{A'B'}(-\vec{p}) = \begin{pmatrix} v^{\dagger}_R(-\vec{p}) \\ v^{\dagger}_L(-\vec{p})\end{pmatrix}\\ \times\delta\mathcal{H}_{A'B'}(\vec{p})[v_R(-\vec{p}), v_L(-\vec{p})].\end{aligned} \tag{A8}$$

This implies that the 2×2 matrices $\Lambda_{A'B'}$, $\tilde{\Lambda}_{A'B'}$ determine the Lorentz-violating effects.

Combining the above results, we obtain the spinor-decomposed Hamiltonian appearing in Eq. (12):

$$\begin{aligned}H_{A'B'}(\vec{p}) &= H^{\dagger}_{B'A'}(\vec{p})\\ &= \delta_{A'B'}\begin{pmatrix} |\vec{p}| & m_{(A')}\eta(\vec{p}) \\ -m_{(A')}\eta^{*}(-\vec{p}) & -|\vec{p}|\end{pmatrix}\\ &\quad + \begin{pmatrix} \Lambda_{A'B'}(\vec{p}) & \tilde{\Lambda}_{A'B'}(\vec{p}) \\ -\tilde{\Lambda}^{*}_{A'B'}(-\vec{p}) & -\Lambda^{*}_{A'B'}(-\vec{p})\end{pmatrix},\end{aligned} \tag{A9}$$

where η is the 2×2 diagonal matrix of phases $\eta(\vec{p}) = -\eta(-\vec{p}) = \mathrm{diag}[\overline{u}_L(\vec{p})v_R(-\vec{p}), \overline{u}_R(\vec{p})v_L(-\vec{p})]$.

We seek an explicit expression for $\Lambda_{A'B'}$. The next subsection shows that the effects of $\tilde{\Lambda}_{A'B'}$ are subleading order, so we concentrate here on the projections in $\Lambda_{A'B'}$, which involve the spinors u_L and u_R. It is useful first to find expressions for the quantities $\overline{u}_{\alpha}\{1, \gamma_5, \gamma^{\mu}, \gamma_5\gamma^{\mu}, \sigma^{\mu\nu}\}u_{\beta}$, where $\alpha, \beta = L, R$. We obtain the following nonzero results:

$$\begin{aligned}\overline{u}_{\alpha}\gamma^{\mu}u_{\beta} &= p^{\mu}\delta_{\alpha\beta}/|\vec{p}|,\\ \overline{u}_{\alpha}\gamma_5\gamma^{\mu}u_{\beta} &= S_{\alpha}p^{\mu}\delta_{\alpha\beta}/|\vec{p}|,\\ \overline{u}_L\sigma^{\mu\nu}u_R &= (\overline{u}_R\sigma^{\mu\nu}u_L)^{*}\\ &= i\sqrt{2}(p^{\mu}(\epsilon_+)^{\nu} - p^{\nu}(\epsilon_+)^{\mu})/|\vec{p}|,\end{aligned} \tag{A10}$$

where $S_L = 1$, $S_R = -1$, $p^{\mu} = (|\vec{p}|; \vec{p})$, and $(\epsilon_+)^{\mu}$ satisfies the relations (15). With these results and Eqs. (A1) and (A2), we can extract the projections of $\delta\mathcal{H}$ onto u_L and u_R:

$$\Lambda_{A'B'}=\frac{1}{|\vec{p}|}\begin{pmatrix}[(a+b)^{\mu}p_{\mu}-(c+d)^{\mu\nu}p_{\mu}p_{\nu}]_{A'B'} & -i\sqrt{2}p_{\mu}(\epsilon_{+})_{\nu}[g^{\mu\nu\sigma}p_{\sigma}-H^{\mu\nu}]_{A'B'}\\ i\sqrt{2}p_{\mu}(\epsilon_{+})^{*}_{\nu}[g^{\mu\nu\sigma}p_{\sigma}-H^{\mu\nu}]_{A'B'} & [(a-b)^{\mu}p_{\mu}-(c-d)^{\mu\nu}p_{\mu}p_{\nu}]_{A'B'}\end{pmatrix}. \tag{A11}$$

In this expression, we neglect off-diagonal terms entering as mass multiplied by coefficients for Lorentz violation, since in most situations these terms are suppressed relative to those above.

2. Block diagonalization

The above spinor decomposition of the Hamiltonian is independent of the specific neutrino mass spectrum. To make further progress, we adopt the scenario described at the beginning of Sec. II B and restrict attention to ultrarelativistic dynamics in the subspace of light neutrinos, spanned by the a' indices. The Hamiltonian is then dominated by the diagonal kinetic term in Eq. (A9). The upper and lower diagonal blocks of this term have opposite sign, so they differ by an amount large compared to both mass and Lorentz-violating terms. This in turn implies that standard perturbation techniques to remove the off-diagonal blocks can be applied. As a result, terms in the off-diagonal blocks of Eq. (A9) appear at second order in the block-diagonalized form. One consequence is that the leading-order mass contribution appears at second order, whereas certain forms of Lorentz violation appear already at first order. This feature can ultimately be traced to the γ-matrix structure of the Lorentz-covariant portion of the theory.

Provided the conditions $m_{(a')},|\Lambda_{a'b'}|,|\tilde{\Lambda}_{a'b'}|\ll|\vec{p}|$ are satisfied, the block diagonalization of Eq. (A9) can proceed through the perturbative construction of an appropriate unitary matrix $\mathcal{U}$. First, write $\mathcal{U}$ in the form $\mathcal{U}=I+\boldsymbol{\epsilon}^{(1)}+\boldsymbol{\epsilon}^{(2)}+\ldots$, where $\boldsymbol{\epsilon}^{(n)}$ is of nth order in the dimensionless small quantities $m_{(a')}/|\vec{p}|$, $\Lambda_{a'b'}/|\vec{p}|$, and $\tilde{\Lambda}_{a'b'}/|\vec{p}|$. The block-diagonal Hamiltonian resulting from this transformation can be expanded in a similar fashion:

$$\begin{aligned}H_{\hat{a}'\hat{b}'}&=\mathcal{U}_{\hat{a}'a'}H_{a'b'}\mathcal{U}^{\dagger}_{\hat{b}'b'}\\&=H^{(0)}_{\hat{a}'\hat{b}'}+H^{(1)}_{\hat{a}'\hat{b}'}+H^{(2)}_{\hat{a}'\hat{b}'}+\cdots,\end{aligned} \tag{A12}$$

where each $H^{(n)}_{\hat{a}'\hat{b}'}$ is nth order in small quantities. The zeroth-order term $H^{(0)}_{\hat{a}'\hat{b}'}$ is the usual kinetic term, which is already block diagonal. The first-order term $H^{(1)}_{\hat{a}'\hat{b}'}$ can be made block diagonal by an appropriate choice of $\boldsymbol{\epsilon}^{(1)}$. A suitable leading-order transformation is

$$\epsilon^{(1)}_{\hat{a}'b'}=\frac{\delta_{\hat{a}'a'}}{2|\vec{p}|}\begin{pmatrix}0 & \hat{\epsilon}_{a'b'}(\vec{p})\\ \hat{\epsilon}^{*}_{a'b'}(-\vec{p}) & 0\end{pmatrix}, \tag{A13}$$

where

$$\hat{\epsilon}_{a'b'}(\vec{p})=m_{(a')}\delta_{a'b'}\,\eta(\vec{p})+\tilde{\Lambda}_{a'b'}(\vec{p}). \tag{A14}$$

Using $\boldsymbol{\epsilon}^{(1)}$ and $H^{(2)}_{\hat{a}'\hat{b}'}$, which depends on both $\boldsymbol{\epsilon}^{(1)}$ and $\boldsymbol{\epsilon}^{(2)}$, we can find $\boldsymbol{\epsilon}^{(2)}$ and then continue iteratively to arbitrary order.

Under the transformation $\mathcal{U}$, the Hamiltonian restricted to light neutrinos may be written

$$H_{\hat{a}'\hat{b}'}=\begin{pmatrix}h_{\hat{a}'\hat{b}'}(\vec{p}) & 0\\ 0 & -h^{*}_{\hat{a}'\hat{b}'}(-\vec{p})\end{pmatrix}. \tag{A15}$$

Calculating $\mathcal{U}$ to second order in small quantities yields the second-order Hamiltonian

$$h_{\hat{a}'\hat{b}'}(\vec{p})=\delta_{\hat{a}'a'}\delta_{\hat{b}'b'}\left[\left(|\vec{p}|+\frac{1}{2|\vec{p}|}m^{2}_{(a')}\right)\delta_{a'b'}+\Lambda_{a'b'}(\vec{p})\right]. \tag{A16}$$

This expression neglects terms that are second order in coefficients for Lorentz violation and terms that enter as the product of $m_{(a')}/|\vec{p}|$ with $\tilde{\Lambda}$. The latter terms constitute subleading-order corrections under the reasonable assumption that Λ and $\tilde{\Lambda}$ are comparable in size.

While formally the two bases related by $\mathcal{U}$ are different, in practice this difference is of little consequence. Our main goal is to determine oscillation probabilities. The effects of $\mathcal{U}$ appear in the mixing matrix and therefore modify the amplitudes of oscillations. However, since $\mathcal{U}$ is close to the identity, the basis change produces only tiny and unobservable changes in oscillation amplitudes. It therefore suffices in practice to assume $\mathcal{U}=I$ for purposes of the basis transformation, corresponding to ignoring the difference between the a' and $\hat{a}'$ indices. Similar arguments apply to the field redefinition relating ν and χ. This also underlies the validity of assuming unitarity mixing matrices in the conventional case with neutrino mass, even though the submatrix $V_{a'a}$ is only approximately unitary. In contrast, the diagonalization of h in Eq. (A16) can introduce arbitrary amounts of mixing.

The above description in the mass-diagonal basis completely determines the neutrino dynamics, but in practical situations a description in the weak-interaction basis is more useful. This requires the transformation of $h_{a'b'}$ to the original flavor basis.

The first step in implementing the desired transformation is to determine the relation between the coefficients in Eq. (2) and those in Eq. (A2). In terms of the unitary matrix $V_{A'A}$, we find

$$
\begin{aligned}
c^{\mu\nu}_{A'B'} &= \mathrm{Re}V_{A'A}V^*_{B'B}(c+d)^{\mu\nu}_{AB},\\
d^{\mu\nu}_{A'B'} &= i\,\mathrm{Im}V_{A'A}V^*_{B'B}(c+d)^{\mu\nu}_{AB},\\
e^{\nu}_{A'B'} &= i\,\mathrm{Im}V_{A'A}V_{B'B}[(e+if)^{\nu}\mathcal{C}]_{AB},\\
if^{\nu}_{A'B'} &= \mathrm{Re}V_{A'A}V_{B'B}[(e+if)^{\nu}\mathcal{C}]_{AB},\\
\frac{1}{2}g^{\lambda\mu\nu}_{A'B'} &= \mathrm{Re}V_{A'A}V_{B'B}\frac{1}{2}(g^{\lambda\mu\nu}\mathcal{C})_{AB}\\
&\quad -\mathrm{Im}V_{A'A}V_{B'B}\frac{1}{4}\epsilon^{\lambda\mu\rho\sigma}(g^{\nu}_{\rho\sigma}\mathcal{C})_{AB},\\
m_{A'B'} &= \mathrm{Re}V_{A'A}V_{B'B}[(m+im_5)\mathcal{C}]_{AB}\equiv m_{(A')}\delta_{A'B'},\\
im_{5A'B'} &= i\,\mathrm{Im}V_{A'A}V_{B'B}[(m+im_5)\mathcal{C}]_{AB}\equiv 0,\\
a^{\nu}_{A'B'} &= i\,\mathrm{Im}V_{A'A}V^*_{B'B}(a+b)^{\nu}_{AB},\\
b^{\nu}_{A'B'} &= \mathrm{Re}V_{A'A}V^*_{B'B}(a+b)^{\nu}_{AB},\\
\frac{1}{2}H^{\mu\nu}_{A'B'} &= i\,\mathrm{Im}V_{A'A}V_{B'B}\frac{1}{2}(H^{\mu\nu}\mathcal{C})_{AB}\\
&\quad +i\,\mathrm{Re}V_{A'A}V_{B'B}\frac{1}{4}\epsilon^{\mu\nu\rho\sigma}(H_{\rho\sigma}\mathcal{C})_{AB}.
\end{aligned}
\tag{A17}
$$

Note that all the coefficients in the mass-diagonal basis are either pure real or pure imaginary, reflecting the Majorana nature of neutrinos in this basis. Using this equation, we obtain

$$
\begin{aligned}
&[(a+b)^{\mu}p_{\mu}-(c+d)^{\mu\nu}p_{\mu}p_{\nu}]_{a'b'}\\
&\quad=[(a+b)^{\mu}p_{\mu}-(c+d)^{\mu\nu}p_{\mu}p_{\nu}]_{ab}V_{a'a}V^*_{b'b},\\
&[(a-b)^{\mu}p_{\mu}-(c-d)^{\mu\nu}p_{\mu}p_{\nu}]_{a'b'}\\
&\quad=[-(a+b)^{\mu}p_{\mu}-(c+d)^{\mu\nu}p_{\mu}p_{\nu}]^*_{ab}V^*_{a'a}V_{b'b},\\
&-i\sqrt{2}p_{\mu}(\epsilon_+)_{\nu}[g^{\mu\nu\sigma}p_{\sigma}-H^{\mu\nu}]_{a'b'}\\
&\quad=-i\sqrt{2}p_{\mu}(\epsilon_+)_{\nu}[(g^{\mu\nu\sigma}p_{\sigma}-H^{\mu\nu})\mathcal{C}]_{ab}V_{a'a}V_{b'b},\\
&i\sqrt{2}p_{\mu}(\epsilon_+)^*_{\nu}[g^{\mu\nu\sigma}p_{\sigma}-H^{\mu\nu}]_{a'b'}\\
&\quad=i\sqrt{2}p_{\mu}(\epsilon_+)^*_{\nu}[(g^{\mu\nu\sigma}p_{\sigma}+H^{\mu\nu})\mathcal{C}]^*_{ab}V^*_{a'a}V^*_{b'b},
\end{aligned}
\tag{A18}
$$

using the assumption that the submatrix $V_{a'a}$ is unitary.

Within a standard seesaw mechanism, the right-handed Majorana-mass matrix R appearing in Eq. (8) is large, $|R| \gg |L|,|D|$. Calculating the matrix V_{AB} at leading order in small mass ratios $|L|/|R|$ and $|D|/|R|$ produces the identity

$$
m_{(a')}\delta_{a'b'} = V_{a'a}V_{b'b}(m_l)_{ab}, \tag{A19}
$$

where $m_l = L - DR^{-1}D^T$, and hence the relation

$$
m^2_{(a')}\delta_{a'b'} = V_{a'a}V^*_{b'b}(m_l m_l^{\dagger})_{ab} = V^*_{a'a}V_{b'b}(m_l m_l^{\dagger})^*_{ab}. \tag{A20}
$$

Combining results yields the desired form

$$
\begin{aligned}
&\left[\left(|\vec{p}| + \frac{1}{2|\vec{p}|}m^2_{(a')}\right)\delta_{a'b'} + \Lambda_{a'b'}(\vec{p})\right]\\
&\quad = \begin{pmatrix} V_{a'a} & 0 \\ 0 & V^*_{a'a} \end{pmatrix}(h_{\mathrm{eff}})_{ab}\begin{pmatrix} V^*_{b'b} & 0 \\ 0 & V_{b'b} \end{pmatrix},
\end{aligned}
\tag{A21}
$$

where h_{eff} is given in Eq. (14).

APPENDIX B: MINIMAL SME TERMS

Restricting attention to the coefficients $(c_L)^{\mu\nu}_{ab}, (a_L)^{\mu}_{ab}$, which are contained in the minimal gauge-invariant SME, effectively decouples neutrinos and antineutrinos and produces vanishing transition probabilities (21c) and (21d). This appendix describes a useful parametrization of these coefficients.

Each coefficient matrix for Lorentz violation can be parametrized with three eigenvalues and a constant unitary matrix. We define

$$
(c_L)^{\mu\nu} = (\hat{U}^{\mu\nu})^{\dagger}\begin{pmatrix} (c_L)^{\mu\nu}_{(1)} & 0 & 0 \\ 0 & (c_L)^{\mu\nu}_{(2)} & 0 \\ 0 & 0 & (c_L)^{\mu\nu}_{(3)} \end{pmatrix}\hat{U}^{\mu\nu} \tag{B1}
$$

for each coefficient matrix $(c_L)^{\mu\nu}$ and

$$
(a_L)^{\mu} = (\hat{U}^{\mu})^{\dagger}\begin{pmatrix} (a_L)^{\mu}_{(1)} & 0 & 0 \\ 0 & (a_L)^{\mu}_{(2)} & 0 \\ 0 & 0 & (a_L)^{\mu}_{(3)} \end{pmatrix}\hat{U}^{\mu} \tag{B2}
$$

for each coefficient matrix $(a_L)^{\mu}$. The unitary diagonalizing matrices $\hat{U}^{\mu\nu}, \hat{U}^{\mu}$ are chosen so that if there is only a single nonvanishing coefficient matrix then U_{eff} in Eq. (19) takes the block-diagonal form

$$
U_{\mathrm{eff}} = \begin{pmatrix} \hat{U} & 0 \\ 0 & \hat{U}^* \end{pmatrix}. \tag{B3}
$$

The reader is warned that the above decomposition is frame dependent, so neither the eigenvalues nor the mixing matrices behave as tensors under observer Lorentz transformations. We therefore advocate restricting this type of decomposition to the standard Sun-centered celestial equatorial frame.

Adopting a CKM-like decomposition of the $\hat{U}$ matrices, we denote mixing angles and phases associated with each $(c_L)^{\mu\nu}$ by $\theta^{\mu\nu}_{12}, \theta^{\mu\nu}_{13}, \theta^{\mu\nu}_{23}$ and $\delta^{\mu\nu}, \beta^{\mu\nu}_1, \beta^{\mu\nu}_2$. Similarly, for each $(a_L)^{\mu}$ we write θ^{μ}_{12}, θ^{μ}_{13}, θ^{μ}_{23}, and $\delta^{\mu\nu}$, β^{μ}_1, β^{μ}_2. The $\hat{U}$ matrices may then be written explicitly in the form

$$\hat{U}^{\mu\nu}=\begin{bmatrix} c_{12}^{\mu\nu}c_{13}^{\mu\nu} & -s_{12}^{\mu\nu}c_{23}^{\mu\nu}-c_{12}^{\mu\nu}s_{23}^{\mu\nu}s_{13}^{\mu\nu}e^{-i\delta^{\mu\nu}} & s_{12}^{\mu\nu}s_{23}^{\mu\nu}-c_{12}^{\mu\nu}c_{23}^{\mu\nu}s_{13}^{\mu\nu}e^{-i\delta^{\mu\nu}} \\ s_{12}^{\mu\nu}c_{13}^{\mu\nu} & c_{12}^{\mu\nu}c_{23}^{\mu\nu}-s_{12}^{\mu\nu}s_{23}^{\mu\nu}s_{13}^{\mu\nu}e^{-i\delta^{\mu\nu}} & -c_{12}^{\mu\nu}s_{23}^{\mu\nu}-s_{12}^{\mu\nu}c_{23}^{\mu\nu}s_{13}^{\mu\nu}e^{-i\delta^{\mu\nu}} \\ s_{13}^{\mu\nu}e^{i\delta^{\mu\nu}} & s_{23}^{\mu\nu}c_{13}^{\mu\nu} & c_{23}^{\mu\nu}c_{13}^{\mu\nu} \end{bmatrix}\begin{bmatrix} 1 & 0 & 0 \\ 0 & e^{i\beta_1^{\mu\nu}} & 0 \\ 0 & 0 & e^{i\beta_2^{\mu\nu}} \end{bmatrix}, \tag{B4}$$

$$\hat{U}^{\mu}=\begin{bmatrix} c_{12}^{\mu}c_{13}^{\mu} & -s_{12}^{\mu}c_{23}^{\mu}-c_{12}^{\mu}s_{23}^{\mu}s_{13}^{\mu}e^{-i\delta^{\mu}} & s_{12}^{\mu}s_{23}^{\mu}-c_{12}^{\mu}c_{23}^{\mu}s_{13}^{\mu}e^{-i\delta^{\mu}} \\ s_{12}^{\mu}c_{13}^{\mu} & c_{12}^{\mu}c_{23}^{\mu}-s_{12}^{\mu}s_{23}^{\mu}s_{13}^{\mu}e^{-i\delta^{\mu}} & -c_{12}^{\mu}s_{23}^{\mu}-s_{12}^{\mu}c_{23}^{\mu}s_{13}^{\mu}e^{-i\delta^{\mu}} \\ s_{13}^{\mu}e^{i\delta^{\mu}} & s_{23}^{\mu}c_{13}^{\mu} & c_{23}^{\mu}c_{13}^{\mu} \end{bmatrix}\begin{bmatrix} 1 & 0 & 0 \\ 0 & e^{i\beta_1^{\mu}} & 0 \\ 0 & 0 & e^{i\beta_2^{\mu}} \end{bmatrix}, \tag{B5}$$

where $s_{ab}^{\mu\nu}=\sin\theta_{ab}^{\mu\nu}$, $c_{ab}^{\mu\nu}=\cos\theta_{ab}^{\mu\nu}$, $s_{ab}^{\mu}=\sin\theta_{ab}^{\mu}$, and $c_{ab}^{\mu}=\cos\theta_{ab}^{\mu}$.

In the conventional massive-neutrino analysis, the β matrix of phases can be absorbed into the amplitudes $b_a(t;\vec{p})$ and $d_a(t;\vec{p})$, so these phases are normally unobservable and can be neglected. However, in the present context, only one set of β phases may be absorbed in this fashion. The presence of multiple coefficient matrices for Lorentz violation implies that they cannot typically be neglected.

Neutrino oscillations are insensitive to terms in the effective Hamiltonian that are proportional to the identity. Consequently, only two eigenvalue differences for each coefficient matrix for Lorentz violation contribute to oscillation effects. Also, each coefficient matrix is associated with three mixing angles and three phases. It follows that the maximum number of gauge-invariant degrees of freedom that enter into neutrino oscillations in the minimal SME alone is 16×8 for c_L and 4×8 for a_L, for a total of 160. However, some of these are unobservable. The 8 trace components $\eta_{\mu\nu}(c_L)^{\mu\nu}$ are Lorentz invariant, and both these and the 6×8-component antisymmetric piece of $(c_L)^{\mu\nu}$ are absent in the leading-order Hamiltonian (14). This leaves 104 leading-order degrees of freedom in a_L and c_L, in agreement with the numbers listed in Table I. For the minimal SME, one set of β phases is also unobservable, which reduces the total number of degrees of freedom to 102.

[1] For recent overviews of various experimental and theoretical approaches to Lorentz and *CPT* violation, see, for example, *CPT and Lorentz Symmetry II*, edited by V.A. Kostelecký (World Scientific, Singapore, 2002).

[2] D. Colladay and V.A. Kostelecký, Phys. Rev. D **55**, 6760 (1997); *ibid.* **58**, 116002 (1998).

[3] V.A. Kostelecký and R. Potting, Phys. Rev. D **51**, 3923 (1995).

[4] V.A. Kostelecký and R. Lehnert, Phys. Rev. D **63**, 065008 (2001).

[5] O.W. Greenberg, Phys. Rev. Lett. **89**, 231602 (2002); Phys. Lett. B **567**, 179 (2003).

[6] V.A. Kostelecký and S. Samuel, Phys. Rev. D **39**, 683 (1989); **40**, 1886 (1989); Phys. Rev. Lett. **63**, 224 (1989); **66**, 1811 (1991).

[7] V.A. Kostelecký and R. Potting, Nucl. Phys. **B359**, 545 (1991); Phys. Lett. B **381**, 89 (1996); Phys. Rev. D **63**, 046007 (2001); V.A. Kostelecký, M. Perry, and R. Potting, Phys. Rev. Lett. **84**, 4541 (2000).

[8] S.M. Carroll *et al.*, Phys. Rev. Lett. **87**, 141601 (2001); Z. Guralnik, R. Jackiw, S.Y. Pi, and A.P. Polychronakos, Phys. Lett. B **517**, 450 (2001); C.E. Carlson, C.D. Carone, and R.F. Lebed, *ibid.* **518**, 201 (2001); A. Anisimov, T. Banks, M. Dine, and M. Graesser, Phys. Rev. D **65**, 085032 (2002); I. Mocioiu, M. Pospelov, and R. Roiban, *ibid.* **65**, 107702 (2002); M. Chaichian, M.M. Sheikh-Jabbari, and A. Tureanu, hep-th/0212259; J.L. Hewett, F.J. Petriello, and T.G. Rizzo, Phys. Rev. D **66**, 036001 (2002).

[9] R. Gambini and J. Pullin, in Ref. [1], J. Alfaro, H.A. Morales-Técotl, L.F. Urrutia, Phys. Rev. D **66**, 124006 (2002); D. Sudarsky, L. Urrutia, and H. Vucetich, Phys. Rev. Lett. **89**, 231301 (2002); Phys. Rev. D **68**, 024010 (2003); G. Amelino-Camelia, Mod. Phys. Lett. A **17**, 899 (2002); Y.J. Ng, *ibid.* **18**, 1073 (2003); R. Myers and M. Pospelov, Phys. Rev. Lett. **90**, 211601 (2003); N.E. Mavromatos, hep-ph/0305215.

[10] C.D. Froggatt and H.B. Nielsen, hep-ph/0211106.

[11] J.D. Bjorken, Phys. Rev. D **67**, 043508 (2003).

[12] KTeV Collaboration, H. Nguyen, in Ref. [1]; OPAL Collaboration, R. Ackerstaff *et al.*, Z. Phys. C **76**, 401 (1997); DELPHI Collaboration, M. Feindt *et al.*, Report No. DELPHI 97-98 CONF 80 1997; BELLE Collaboration, K. Abe *et al.*, Phys. Rev. Lett. **86**, 3228 (2001); BaBar Collaboration, B. Aubert *et al.*, hep-ex/0303043; FOCUS Collaboration, J.M. Link *et al.*, Phys. Lett. B **556**, 7 (2003).

[13] D. Colladay and V.A. Kostelecký, Phys. Lett. B **344**, 259 (1995); Phys. Rev. D **52**, 6224 (1995); Phys. Lett. B **511**, 209 (2001); V.A. Kostelecký and R. Van Kooten, Phys. Rev. D **54**, 5585 (1996); O. Bertolami *et al.*, Phys. Lett. B **395**, 178 (1997); V.A. Kostelecký, Phys. Rev. Lett. **80**, 1818 (1998); Phys. Rev. D **61**, 016002 (2000); **64**, 076001 (2001); N. Isgur *et al.*, Phys. Lett. B **515**, 333 (2001).

[14] L.R. Hunter *et al.*, in *CPT and Lorentz Symmetry*, edited by V.A. Kostelecký (World Scientific, Singapore, 1999); D. Bear *et al.*, Phys. Rev. Lett. **85**, 5038 (2000); D.F. Phillips *et al.*, Phys. Rev. D **63**, 111101 (2001); M.A. Humphrey *et al.* (to be

published) physics/0103068; **62**, 063405 (2000); V.A. Kostelecký and C.D. Lane, Phys. Rev. D **60**, 116010 (1999); J. Math. Phys. **40**, 6245 (1999).
[15] R. Bluhm *et al.*, Phys. Rev. Lett. **88**, 090801 (2002); Phys. Rev. D **68**, 125008 (2003).
[16] F. Canè *et al.*, physics/0309070.
[17] H. Dehmelt *et al.*, Phys. Rev. Lett. **83**, 4694 (1999); R. Mittleman *et al.*, *ibid.* **83**, 2116 (1999); G. Gabrielse *et al.*, *ibid.* **82**, 3198 (1999); R. Bluhm *et al.*, *ibid.* **82**, 2254 (1999); **79**, 1432 (1997); Phys. Rev. D **57**, 3932 (1998).
[18] B. Heckel, in Ref. [1]; L.-S. Hou, W.-T. Ni, and Y.-C.M. Li, Phys. Rev. Lett. **90**, 201101 (2003); R. Bluhm and V.A. Kostelecký, *ibid.* **84**, 1381 (2000).
[19] S.M. Carroll, G.B. Field, and R. Jackiw, Phys. Rev. D **41**, 1231 (1990); V.A. Kostelecký and M. Mewes, Phys. Rev. Lett. **87**, 251304 (2001).
[20] R. Jackiw and V.A. Kostelecký, Phys. Rev. Lett. **82**, 3572 (1999); C. Adam and F.R. Klinkhamer, Nucl. Phys. **B657**, 214 (2003); H. Müller, C. Braxmaier, S. Herrmann, A. Peters, and C. Lämmerzahl, Phys. Rev. D **67**, 056006 (2003); T. Jacobson, S. Liberati, and D. Mattingly, *ibid.* **67**, 124011 (2003); V.A. Kostelecký, R. Lehnert, and M. Perry, Phys. Rev. D **68**, 123511 (2003); V.A. Kostelecký and A.G.M. Pickering, Phys. Rev. Lett. **91**, 031801 (2003); R. Lehnert, Phys. Rev. D **68**, 085003 (2003); G.M. Shore, gr-qc/0304059.
[21] J. Lipa *et al.*, Phys. Rev. Lett. **90**, 060403 (2003); H. Müller *et al.*, *ibid.* **91**, 020401 (2003).
[22] V.A. Kostelecký and M. Mewes, Phys. Rev. D **66**, 056005 (2002).
[23] V.W. Hughes *et al.*, Phys. Rev. Lett. **87**, 111804 (2001); R. Bluhm *et al.*, *ibid.* **84**, 1098 (2000).
[24] S. Coleman and S. L. Glashow, Phys. Rev. D **59**, 116008 (1999).
[25] V. Barger, S. Pakvasa, T.J. Weiler, and K. Whisnant, Phys. Rev. Lett. **85**, 5055 (2000).
[26] J.N. Bahcall, V. Barger, and D. Marfatia, Phys. Lett. B **534**, 114 (2002).
[27] A. de Gouvêa, Phys. Rev. D **66**, 076005 (2002).
[28] I. Mocioiu and M. Pospelov, Phys. Lett. B **537**, 114 (2002).
[29] V.A. Kostelecký and M. Mewes, Phys. Rev. D (to be published), hep-ph/0308300.
[30] R. Brustein, D. Eichler, and S. Foffa, Phys. Rev. D **65**, 105006 (2002).
[31] A survey of the available data is provided by The Particle Data Group, K. Hagiwara *et al.*, Phys. Rev. D **66**, 010001 (2002).
[32] KATRIN Collaboration, A. Osipowicz *et al.*, hep-ex/0109033.
[33] See, for example, P. Vogel in Ref. [31].
[34] K. Hirata *et al.*, Phys. Rev. Lett. **58**, 1490 (1987); R.M. Bionta *et al.*, *ibid.* **58**, 1494 (1987).
[35] L. Wolfenstein, Phys. Rev. D **17**, 2369 (1978); S. Mikheev and A. Smirnov, Sov. J. Nucl. Phys. **42**, 913 (1986); Sov. Phys. JETP **64**, 4 (1986); Nuovo Cimento Soc. Ital. Fis., C **C9**, 17 (1986).
[36] Super-Kamiokande Collaboration, S. Fukuda *et al.*, Phys. Rev. Lett. **81**, 1562 (1998); **82**, 2644 (1999); **85**, 3999 (2000).
[37] B.T. Cleveland *et al.*, Astrophys. J. **496**, 505 (1998).
[38] GALLEX Callaboration, W. Hampel *et al.*, Phys. Lett. B **447**, 127 (1999).
[39] GNO Collaboration, M. Altmann *et al.*, Phys. Lett. B **490**, 16 (2000).
[40] SAGE Collaboration, J.N. Abdurashitov *et al.*, J. Exp. Theor. Phys. **95**, 181 (2002).
[41] Super-Kamiokande Collaboration, S. Fukuda *et al.*, Phys. Rev. Lett. **86**, 5651 (2001); **86**, 5656 (2001); Phys. Lett. B **539**, 179 (2002).
[42] SNO Collaboration, Q.R. Ahmad *et al.*, Phys. Rev. Lett. **87**, 071301 (2001); **89**, 011301 (2002); **89**, 011302 (2002).
[43] KamLAND Collaboration, K. Eguchi *et al.*, Phys. Rev. Lett. **90**, 021802 (2003).
[44] LSND Collaboration, C. Athanassopoulos *et al.*, Phys. Rev. Lett. **81**, 1774 (1998); LSND Collaboration, A. Aguilar *et al.*, Phys. Rev. D **64**, 112007 (2001).
[45] K2K Collaboration M.H. Ahn *et al.*, Phys. Rev. Lett. **90**, 041801 (2003).
[46] For comprehensive reviews of conventional neutrino physics see, for example, F. Boehm and P. Vogel, *Physics of Massive Neutrinos*, 2nd ed. (Cambridge University Press, Cambridge, 1992); R.N. Mohapatra and P.B. Pal, *Massive Neutrinos in Physics and Astrophysics*, 3rd ed. (World Scientific, Singapore, 2002).
[47] For recent reviews of theoretical aspects of neutrino masses and mixings see, for example, R. Mohapatra, hep-ph/0211252; S.M. Bilenky, C. Giunti, J.A. Grifols, and E. Masso, Phys. Rep. **379**, 69 (2003).
[48] M. Gell-Mann, P. Ramond, and R. Slansky, in *Supergravity*, edited by P. van Nieuwenhuizen and D.Z. Freedman (North Holland, Amsterdam, 1979); T. Yanagida, in *Workshop on Unified Theory and the Baryon Number of the Universe*, edited by O. Sawada and A. Sugamoto, KEK, Japan, 1979; R. Mohapatra and G. Senjanović, Phys. Rev. Lett. **44**, 912 (1980), a recent review of the seesaw literature with discussion of alternatives to the standard form is given in P. Langacker, hep-ph/0304053.
[49] D. Colladay and P. McDonald, J. Math. Phys. **43**, 3554 (2002).
[50] M.S. Berger and V.A. Kostelecký, Phys. Rev. D **65**, 091701(R) (2002).
[51] For a review see, for example, T.K. Kuo and J. Pantaleone, Rev. Mod. Phys. **61**, 937 (1989).
[52] J.N. Bahcall, M.H. Pinsonneault, and S. Basu, Astrophys. J. **555**, 990 (2001).
[53] For a detailed discussion in the Lorentz-conserving case, see, for example, M. Jacobson and T. Ohlsson, Phys. Rev. D (to be published), hep-ph/0305064.
[54] Note that the energy dependence of these five quantities means they cannot be regarded as conventional mass differences.
[55] G. Barenboim and J. Lykken, Phys. Lett. B **554**, 73 (2003).
[56] The precise definitions of the Sun-centered frame and of a standard Earth-based frame appropriate for terrestrial experiments are given in Ref. [22], along with the form of the transformation relating them.
[57] V.A. Kostelecký, C.D. Lane, and A.G.M. Pickering, Phys. Rev. D **65**, 056006 (2002).
[58] B. Achkar *et al.*, Phys. Lett. B **374**, 243 (1996).
[59] M. Apollonio *et al.*, Phys. Lett. B **466**, 415 (1999).
[60] G. Zacek *et al.*, Phys. Rev. D **34**, 2621 (1986).
[61] F. Boehm *et al.*, Phys. Rev. D **64**, 112001 (2001).
[62] L. Borodovsky *et al.*, Phys. Rev. Lett. **68**, 274 (1992).

[63] A. Romosan *et al.*, Phys. Rev. Lett. **78**, 2912 (1997).
[64] CHORUS Collaboration E. Eskut *et al.*, Phys. Lett. B **497**, 8 (2001).
[65] NOMAD Collaboration P. Astier *et al.*, Nucl. Phys. **B611**, 3 (2001).
[66] NOMAD Collaboration P. Astier *et al.*, Phys. Lett. B **B570**, 19 (2003).
[67] S. Avvakumov *et al.*, Phys. Rev. Lett. **89**, 011804 (2002).
[68] KARMEN Collaboration B. Armbruster *et al.*, Phys. Rev. D **65**, 112001 (2002).
[69] E. Church *et al.*, "*A proposal for an experiment to measure* $\nu_\mu \to \nu_e$ *oscillations and* ν_μ *disappearance at the Fermilab Booster: BooNE*," Fermilab Report No. FERMILAB-P-0898, 1997.
[70] ICARUS Collaboration, "*The ICARUS Experiment: A Second-Generation Proton Decay Experiment and Neutrino Observatory at the Gran Sasso Laboratory*," Report No. LNGS-P28/2001, LNGS-EXP 13/89 add.1/01, ICARUS-TM/2001-03, 2001.
[71] MINOS Collaboration, "*MINOS Technical Design Report*," Fermilab Report No. NuMI-L-337, 1998.
[72] OPERA Collaboration, "*OPERA: An appearance experiment to search* $\nu_\mu \to \nu_\tau$ *oscillations in the CNGS beam*," Report No. CERN/SPSC 2000-028, SPSC/P318, LNGS P25/2000, 2000.
[73] See, for example, M. Honda *et al.*, Phys. Rev. D **52**, 4985 (1995).
[74] G.L. Fogli *et al.*, Phys. Rev. D **60**, 053006 (1999); P. Lipari and M. Lusignoli, *ibid.* **60**, 013003 (1999); R. Foot, C.N. Leung, and O. Yasuda, Phys. Lett. B **443**, 185 (1998).
[75] This example exhibits maximal mixing at $\Theta = 90°$, but it is straightforward to generate Θ-dependent examples with maximal mixing at $\Theta = 0°, 180°$. See Ref. [29].
[76] Note that this behavior may also result from direction dependence or from resonances in h_{eff} at intermediate energy scales.
[77] M.J. Longo, Phys. Rev. D **36**, 3276 (1987); Phys. Rev. Lett. **60**, 173 (1988).
[78] W.D. Arnett and J.L. Rosner, Phys. Rev. Lett. **58**, 1906 (1987).